

National Technical University of Athens
School of Naval Architecture and Marine Engineering



DEVELOPMENT OF A MATHEMATICAL MODEL FOR THE PREDICTION OF SHIP
PROPULSION WITH WIND-ASSISTED SYSTEMS

THESIS OF
MOUSGAS MARINOS

SUPERVISOR: NIKOLAOS THEMELIS, ASSOCIATE PROFESSOR

ATHENS, OCTOBER 2025

Abstract

The maritime industry faces increasing pressure to reduce greenhouse gas emissions and improve energy efficiency in accordance with the International Maritime Organization's (IMO) decarbonization targets. To meet these objectives, ship operators are exploring technologies that reduce fuel consumption and environmental impact. Among the most promising measures are Wind-Assisted Propulsion (WASP) systems, which harness renewable wind energy to support conventional propulsion. This thesis aims to assess the impact of such technologies on fuel consumption and emission reduction, with a specific focus on the suction-based eSAIL system applied to a bulk carrier case study.

The work introduces a computation model, with formulas that could be applied to real operating conditions. The main resistance components established in the methodology—calm-water resistance, added resistance from wind and waves, additional resistances from drift and rudder deflection—are linked through propeller open-water characteristics to determine propulsion power and fuel consumption.

A series of computational analyses were carried out to evaluate ship performance and fuel consumption under varying wind conditions. The results showed that the integration of the suction-based eSAIL system can lead to fuel savings of up to 40 % in a realistic sea-going scenario, corresponding to typical service speed and wind conditions. Additional scenarios were introduced for different sea states, demonstrating that system could be beneficial across a wide range of environmental conditions.

These outcomes demonstrate the strong potential of wind-assisted propulsion systems to reduce fuel consumption and emissions, contributing to the ongoing decarbonisation of maritime transport. Overall, this study highlights that the further development and practical adoption of WASP could play a key role in achieving a more energy-efficient and sustainable future for the shipping industry.

Περίληψη

Η ναυτιλιακή βιομηχανία αντιμετωπίζει αυξανόμενες πιέσεις για τη μείωση των εκπομπών αερίων του θερμοκηπίου και τη βελτίωση της ενεργειακής απόδοσης, σύμφωνα με τους στόχους απανθρακοποίησης του Διεθνούς Ναυτιλιακού Οργανισμού (IMO). Για την επίτευξη αυτών των στόχων, οι πλοιοκτήτες και διαχειριστές στρέφονται σε τεχνολογίες που μειώνουν την κατανάλωση καυσίμου και το περιβαλλοντικό αποτύπωμα. Ανάμεσα στις πιο υποσχόμενες λύσεις συγκαταλέγονται τα Συστήματα Πρόωσης με Βοήθεια Ανέμου (Wind-Assisted Ship Propulsion – WASP), τα οποία αξιοποιούν την ανανεώσιμη αιολική ενέργεια για την υποστήριξη της συμβατικής πρόωσης. Η παρούσα εργασία αποσκοπεί στην αξιολόγηση της επίδρασης αυτών των τεχνολογιών στην κατανάλωση καυσίμου και στη μείωση των εκπομπών, με ειδική έμφαση στο σύστημα αναρρόφησης eSAIL, το οποίο εφαρμόστηκε σε πλοίο μεταφοράς χύδην φορτίου (bulk carrier) ως μελέτη περίπτωσης.

Η εργασία παρουσιάζει ένα υπολογιστικό μοντέλο, με τύπους που μπορούν να εφαρμοστούν σε πραγματικές συνθήκες λειτουργίας. Τα κύρια συστατικά της αντίστασης που καθορίστηκαν στη μεθοδολογία — η αντίσταση σε ήρεμο νερό, η πρόσθετη αντίσταση λόγω ανέμου και κυματισμού, καθώς και οι πρόσθετες αντιστάσεις που προκύπτουν από την πλαγιολίσθηση και την εκτροπή του πηδαλίου — συνδέονται μέσω των χαρακτηριστικών ανοιχτής λειτουργίας (open-water) της προπέλας, ώστε να προσδιοριστεί η απαιτούμενη ισχύς πρόωσης και η κατανάλωση καυσίμου.

Πραγματοποιήθηκαν υπολογιστικές αναλύσεις για την εκτίμηση της απόδοσης του πλοίου και της κατανάλωσης καυσίμου υπό διαφορετικές συνθήκες ανέμου. Τα αποτελέσματα έδειξαν ότι η ενσωμάτωση του συστήματος eSAIL μπορεί να οδηγήσει σε εξοικονόμηση καυσίμου έως και 40 % σε ρεαλιστικό σενάριο πλεύσης, που αντιστοιχεί σε τυπική ταχύτητα υπηρεσίας και πραγματικές συνθήκες ανέμου. Επιπλέον, εξετάστηκαν διαφορετικές καταστάσεις θάλασσας, αποδεικνύοντας ότι το σύστημα μπορεί να είναι ωφέλιμο σε ένα ευρύ φάσμα περιβαλλοντικών συνθηκών.

Τα αποτελέσματα αυτά καταδεικνύουν τη σημαντική δυνατότητα των συστημάτων πρόωσης με υποβοήθηση ανέμου να μειώσουν την κατανάλωση καυσίμου και τις εκπομπές, συμβάλλοντας στη συνεχιζόμενη απανθρακοποίηση της ναυτιλίας. Συνολικά, η μελέτη υπογραμμίζει ότι η περαιτέρω ανάπτυξη και πρακτική εφαρμογή των συστημάτων WASP θα μπορούσε να διαδραματίσει καθοριστικό ρόλο στην επίτευξη μιας πιο ενεργειακά αποδοτικής και βιώσιμης ναυτιλίας στο μέλλον.

Acknowledgements

With the completion of this thesis, I would like to express my gratitude to all who supported me and contributed in different ways to this effort.

First, I would like to sincerely thank my supervisor, [Nikolaos Themelis], for his guidance, trust, and continuous support throughout this project.

His valuable advice, constructive feedback, and deep knowledge were essential for the development and successful completion of this thesis.

Special thanks to all my friends and colleagues for their encouragement and support during the challenges of this journey.

Finally, my deepest gratitude goes to my family. Their unwavering support, patience, and love have been the driving force that guided me to complete my studies and accomplish this thesis.

Contents

Abstract.....	2
Περίληψη	3
Acknowledgements	4
Contents	5
List of Figures.....	7
List of Tables	9
List of Symbols	10
Chapter 1: Introduction	13
1.1 Motivation of the Thesis.....	13
1.2 Purpose and Objectives of the Thesis.....	14
1.3 Structure of the Thesis.....	15
Chapter 2: Literature Review.....	16
2.1 Wind-Assisted Ship Propulsion Systems	17
2.1.1 Flettner Rotors:	17
2.1.2 Kite Sails:.....	18
2.1.3 Rigid Sails.....	18
2.1.4 Suction Sails.....	19
2.2 Review of Works for WASP Performance Assessment.....	20
2.3 Suction-Based Sail System – eSAIL	21
2.3.1 Basic Working Principles	22
2.3.2 Performance Analysis and Application	24
2.3.3 Application in Thesis Modeling.....	24
Chapter 3: Theoretical Model and Methodology.....	25
3.1 Methodology Overview.....	25
3.2 Components of Ship Resistance	27
3.2.1 Calm-Water Resistance (R_{cw}).....	27
3.2.2 Added aerodynamic resistance due to wind.....	28
3.2.3 Added resistance in waves	30
3.2.4 Drift & Rudder Resistance.....	32
3.2.5 WASP thrust contribution.....	37

3.3 Propeller and Engine Performance.....	38
3.3.1 Propeller Open Water Performance and Working Point.....	38
3.3.2 Delivered Power and Main Engine Load.....	40
3.3.3 Wind-Assisted Power Integration.....	40
3.4 Fuel Consumption Model.....	41
Chapter 4: Case Study.....	42
4.1 Ship's Particulars.....	42
4.2 eSAIL Description and Data Source	43
4.2.1 Defined Scenarios	46
4.3 Resistance Components	47
4.3.1 Resistance from Model Tests.....	47
4.3.2 Added Wind Resistance.....	48
4.3.3 Wave Resistance Calculation.....	52
4.3.4. Drift & Rudder resistance	54
4.4 Total Resistance for Defined Scenarios	57
4.5 Power Requirements for Defined Scenarios	61
4.6 Specific Fuel Oil Consumption	62
4.7 Fuel Consumption Comparison.....	63
4.8 Fuel Savings in Different Sea States	65
Chapter 5: Conclusions and Future Research	69
5.1 Main Conclusions of the Thesis	69
5.2 Relation to Previous Studies.....	70
5.3 Future Research Directions	71
References.....	72
Appendix A: Ship Data from Towing Tank Test Report.....	76
Appendix B: Added resistances	77

List of Figures

Figure 1: E-Ship 1 equipped with four Flettner rotors [53]	17
Figure 2: Kite Sail on ship	18
Figure 3: Berge Olympus fitted with four Rigid sails [54].....	18
Figure 4: eSAIL system retrofitted in vessel Bow Olympus [56]	19
Figure 5: Suction sail example [32]	21
Figure 6: Suction sail inactive [32].....	22
Figure 7: Suction sail active [32]	23
Figure 8: Suction sail active with appropriate rotation [32]	23
Figure 9: Methodology Flowchart	26
Figure 10: Sign convention [23]	29
Figure 11: Sign convention for wind directions [23].....	29
Figure 12: System of coordinates	32
Figure 13: Intersection of hull demand thrust coefficient curve and propeller open water performance curve for an example vessel [59]].....	39
Figure 14: eSAIL model 2	43
Figure 15: Position of eSAIL units on the ship's main deck	44
Figure 16: Relative variation of eSAIL effective Forces and Power Consumption under Variable Apparent Wind Speed	45
Figure 17: Relative variation of eSAIL effective Forces and Power Consumption under Constant Apparent Wind Speed.....	46
Figure 18: Resistance in calm water for Scantling draft [49]	47
Figure 19: Wind Resistance Coefficient C_{DA} versus Wind Incidence Angle - Baseline Vessel	49
Figure 20: Wind Resistance Coefficient C_{DA} versus Wind Incidence Angle - eSAIL Fitted Vessel.....	49
Figure 21: Apparent Wind Speed versus Wind Direction for Variable and Constant (U_a) Scenarios.....	50
Figure 22: Lateral Force coefficient (C_Y) versus Wind Incidence Angle.....	51
Figure 23: Yaw Moment coefficient (C_N) versus Wind Incidence Angle	51
Figure 24: Max. Added Resistance in Waves across Peak Period Range ($T_p = 6-15$ s)	53
Figure 25: Variation of Drift Angle with Wind Direction under Different Apparent Wind Conditions for Baseline and eSAIL-Fitted Vessel.....	54
Figure 26: Variation of Rudder Angle with Wind Direction under Different Apparent Wind Conditions for Baseline and eSAIL-Fitted Vessel.....	55
Figure 27: Rudder and Drift Resistance versus Wind Direction under Different Apparent Wind Conditions for Baseline and eSAIL-Fitted Vessel.....	56
Figure 28: Total Resistance Components for Scenario 1 – Variable U_a , No eSAIL.....	57
Figure 29: Total Resistance Components for Scenario 2 – Constant U_a , No eSAIL	58
Figure 30: Total Resistance Components for Scenario 3 – Variable U_a , With eSAIL	58

Figure 31: Total Resistance Components for Scenario 4 – Constant U_a , With eSAIL	59
Figure 32: Total Resistance versus Wave/Wind Direction under Different Apparent Wind Conditions for Baseline and eSAIL-Fitted Vessel.....	60
Figure 33: Total Required Power versus Wave/Wind Direction under Different Apparent Wind Conditions for Baseline and eSAIL-Fitted Vessel.....	61
Figure 34: Specific Fuel Oil Consumption versus Engine load.....	62
Figure 35: Total Daily Fuel Consumption versus Wave/Wind Direction under Different Apparent Wind Conditions for Baseline and eSAIL-Fitted Vessel	63
Figure 36: Fuel Savings in (%) versus Wave/Wind Direction under Different Apparent Wind Conditions for Baseline and eSAIL-Fitted Vessel.....	64
Figure 37: Polar Plot of Fuel Savings across Wave/Wind Angles under Beaufort 4 (Moderate Breeze) Conditions for Baseline and eSAIL-Fitted Vessel	66
Figure 38: Polar Plot of Fuel Savings across Wave/Wind Angles under Beaufort 6 (Strong Breeze) Conditions for Baseline and eSAIL-Fitted Vessel	67
Figure 39: Combined Polar Plot of Fuel Savings across Wave/Wind Angles for Different Sea States (Beaufort 4 and 6) under Baseline and eSAIL-Fitted Conditions	68
Figure 40: Input parameters for regression formula by Fujiwara	78
Figure 41: Lengths L_R, L_E and angles E_1, E_2 [38, Fig. 15]	81

List of Tables

Table 1: Principal Particulars of Ship	42
Table 2: Required data in Scantling draft	48
Table 3: Parameters for calculation of wave resistance.....	52
Table 4: Specific Fuel Oil Consumption versus Engine load.....	62
Table 5: Beaufort Scale of Wind – Representative Sea States [ITTC, 2021 Sea Trials].....	65
Table 6: Properler open-water characteristics in Scantling Draft.....	76
Table 7: Self Propulsion factors for Scantling Draft	76
Table 8: Non-dimensional parameters [23, Tbl. F-2]	78
Table 9: Each coefficient of independent variables	80

List of Symbols

Symbol	Description
AR_h	Underwater portion of the hull's effective aspect ratio
AR_r	Effective aspect ratio
A_r	Rudder area
A_{OD}	Projected lateral area of superstructures on deck (above waterline)
A_{XV}	Area of maximum transverse section exposed to wind.
A_{YV}	Projected lateral area above the waterline.
B	Ship breadth
C_B	Hull block coefficient
C_{DA}	Wind resistance coefficient
C_K	Roll moment coefficient
C_{mc}	Longitudinal lever of the centre of lateral area (from midship)
c_{mean}	Mean chord
C_N	Yaw moment coefficient
C_n	Propeller speed correction factor
C_p	Delivered power correction factor
C_X	Surge force coefficient
c_{XD}	drift-related non-dimensionalized additional resistance
C_Y	Sway (lateral) force coefficient
D	Propeller diameter
DF	Longitudinal effective force
F_{NX}	Rudder resistance
F_{NY}	Lateral rudder force
F_S	Sails lateral force
F_Y	Aerodynamic lateral force
g	Gravitational acceleration
H_{br}	Height of bridge/superstructure top
H_c	Height of the centre of lateral area above waterline
HF	Perpendicular effective force
H_s	Significant wave height
J	Propeller advance coefficient.
k_Q	Propeller torque coefficient
k_T	Propeller thrust coefficient.
k_{yy}	Longitudinal radius of gyration in pitch
L_{BP}	Length between perpendiculars
Loa	Length overall
L_{WL}	Length of waterline
MCR	Maximum Continuous Rating
$m_{fuel, baseline}$	Main engine fuel consumption rate
$m_{fuel, total}$	Total fuel consumption rate
$m_{fuel, WASP}$	Fuel consumption rate for WASP auxiliary load
N	Aerodynamic moment
N_H	Yaw moment by hull
N_{hyd}	Hydrodynamic moment

N_R	Rudder-induced moment
N_{sail}	Moment by sails
n_{MCR}	Engine speed at MCR (rpm).
n_0	propeller speed
P_{con}	eSAIL power consumption (per unit)
P_d	Delivered power
P_{MCR}	Main engine maximum continuous rating power
$P_{MCR ME, lim}$	Limited PMCR for main engine
P_{req}	Total required propulsion power
P_{WASP}	Total required power of WASP
Q_0	Propeller torque
Q_d	Delivered torque
R_{AW}	Added resistance in regular waves
\bar{R}_{aw}	Added resistance in irregular waves
R_{AWM}	Wave reflection added resistance
R_{AWR}	Ship motion added resistance
R_{cw}	Calm-water resistance.
R_T	Total ship resistance
$SFOC$	Specific Fuel Oil Consumption for main engine
$SFOC_{AE}$	Specific Fuel Oil Consumption for auxiliary engines
T_a	Aft draft
t	Thrust deduction factor.
T_f	Fore draft
T_0	Open-water thrust
T_p	Spectral peak period
U_a	Apparent wind speed
U_t	True wind speed
v'	Drift dimensionless speed
v	y-direction ship velocity
u	x-direction ship velocity
V_S	Ship speed
V_0	Propeller advance speed
w	Wake fraction.
X_D	Drift resistance
x_s	Sails level arm
Y'_v, Y''_v	Lateral force's hydrodynamic derivatives
α	Wave heading angle
α_H	ratio of the force on the hull by the rudder to the rudder force
β	Drift angle
γ	peak shape factor.
δ	Rudder angle
$\zeta\alpha$	Wave amplitude
η_0	Propeller open-water efficiency.
η_R	Rotative efficiency.
η_S	Shaft/transmission efficiency.
μ	Smoothing range

ρ_a	Air density
σ	JONSWAP spectral width parameter.
ψ	true wind angle
$\psi\alpha$	apparent wind angle
ω	Angular frequency
ωp	Spectral peak angular frequency

Chapter 1: Introduction

Shipping has long been one of the main pillars of global trade and the international economy. For centuries, ships have carried people and goods across seas and oceans, which also encouraged cultural exchange. Even today, more than 80% of global trade is transported by sea. This shows that shipping is not only an essential part of economic activity but also one of the most important services for society as a whole.

At the same time, the growth of shipping has also brought new challenges, especially concerning its impact on the environment. Modern ships still depend heavily on fossil fuels, which makes them a major contributor to greenhouse gas emissions. Because of this, the international community now calls for cleaner and more sustainable alternatives for ship propulsion [10], [20], [21]. Responding to this imperative, the thesis is driven by the potential of innovative technologies, such as Wind-Assisted Propulsion Systems, that have now re-emerged as sustainable alternative solutions. By integrating theoretical concepts with computational tools, the goal is to demonstrate how such systems could modify a ship's energy profile and reduce its environmental footprint [11], [29].

1.1 Motivation of the Thesis

The maritime industry is entering a critical phase in its transition toward cleaner and more efficient operations. Reducing emissions has become a core objective, driven by stricter international regulations and the increasing demand for sustainable transport. Achieving these targets requires not only policy measures but also practical technological solutions capable of delivering measurable results.

New technologies play a central role in this transition because regulations alone are insufficient without practical solutions to lower fuel use and emissions. Current developments include alternative fuels such as LNG, hydrogen, and ammonia, as well as improvements in engine performance, hull design, and digital route optimization [2], [3]. Among these, wind-assisted propulsion is attracting renewed attention because it is renewable, clean, and cost-effective. Such systems can reduce fuel consumption by harnessing wind energy, often without requiring major changes to ship design or daily operations [1], [8].

However, adopting new technologies involves more than just technical considerations. Shipping companies must also evaluate economic, operational, and organizational factors, including costs, maintenance, crew training, and safety. Systems like those based on wind-assisted propulsion aim to balance theory with practicality, offering real energy savings while remaining usable in everyday conditions. With growing regulatory pressure and rapid technological development, these systems are now at a promising stage. Researchers need to study their performance in depth to guide investment and adoption [11], [17], [23].

Using such technologies does more than improve operations—it also promotes innovation and sustainability, values that are increasingly important for regulators, customers, and investors. Many companies have already started implementing these systems and are supporting further research and development, which strengthens their competitive advantage [23], [33]. In conclusion, there is a strong link between emission reduction frameworks and technological innovation. Regulations set the goals, while wind-assisted systems provide the tools to achieve them. Joint progress in policy, innovation, and simulation will create the foundation for a more sustainable shipping industry, guided by both science and practice. This thesis applies these principles by simulating WASP systems to evaluate their effect on emissions and operational efficiency in real-world conditions [1], [29].

1.2 Purpose and Objectives of the Thesis

The main purpose of this thesis is to assess how suction-based sail systems contribute to ship performance and sustainability through mathematical modeling. Using MATLAB as a computational environment, the work focuses on developing and applying a set of mathematical formulations that describe the aerodynamic and hydrodynamic behavior of a vessel equipped with such a system. The goal is to quantify the potential reduction in fuel consumption and engine load that can be achieved through wind-assisted propulsion [32]. The study aims to translate theoretical knowledge on aerodynamics, propulsion, and resistance into a practical analytical framework. The suction sail system is first described to provide a clear understanding of its operating principle and its role within the overall propulsion balance of the ship. Although the concept is based on well-known physical laws, its technological implementation is relatively new to maritime applications; therefore, presenting its function and interaction with vessel resistance is essential for the subsequent analysis [14].

The second objective is to evaluate the system's performance across different operational conditions, such as wind speed and direction, to determine when suction-based sails offer the highest efficiency. Comparing the results across these conditions helps reveal when and where these systems are most effective and could be better utilized [15].

Finally, the thesis aims to demonstrate how such modeling can support decision-making in ship design and operation. By establishing a reproducible framework, it provides a scientific basis for evaluating wind-assisted technologies and contributes to ongoing research in sustainable maritime propulsion [DNV, 2024].

1.3 Structure of the Thesis

This thesis is structured to progress from the general context of maritime decarbonization to its practical implementation, through the development and analytical evaluation of a computational model focused on suction-based sail systems.

Chapter 1 introduces the subject, explains the aim and objectives, and discusses the need for emission reduction in shipping through new technologies. It highlights the relevance of emission reduction in shipping and the role of innovative technologies such as wind-assisted propulsion, establishing the framework for the study.

Chapter 2 presents a detailed literature review. It covers international regulations from the International Maritime Organization, existing energy-saving systems, and studies on suction-based sail performance compared with other propulsion methods. This chapter provides the theoretical foundation and context required for the following research.

Chapter 3 develops the theoretical framework used to assess the impact of wind-assisted propulsion on ship performance. It presents the formulas that can be utilized for the calculation of the main resistance components, establishing their connection to propulsion power and fuel consumption. The structure of the complete modelling process is summarized through a flowchart illustrating the sequence of computational steps.

Chapter 4 presents the application of the developed theoretical model to the case study vessel and analyses the main findings from the results. The chapter includes the evaluation of total resistance, required power, and fuel consumption under different apparent wind conditions and sea states. The performance of the vessel with and without the eSAIL system is compared across the defined operational scenarios, highlighting the potential fuel reduction, through wind-assisted propulsion.

Chapter 5 presents the conclusions drawn from the overall analysis and summarises the key findings of the research. The results are discussed in relation to existing studies and established theoretical principles, providing context for the outcomes of the developed model. The chapter also outlines proposed directions for future research and highlights the contribution of suction-based wind-assisted propulsion as a promising solution for improving ship efficiency and reducing emissions.

Chapter 2: Literature Review

The shipping industry is undergoing significant change due to climate-related pressures and stricter environmental rules. According to the IMO's GHG study (2011), ships are responsible for about 2.89% of global greenhouse gas emissions, making them a key focus of decarbonization. The International Maritime Organization (IMO) is the main regulatory authority for international shipping and has introduced a series of measures to improve energy efficiency and lower fleet-wide emissions (IMO, 2011).

At the heart of this regulatory approach is the Initial IMO GHG Strategy, adopted in 2018. Its long-term vision is to cut total annual GHG emissions from international shipping by at least 50% by 2050, compared with 2008 levels, while working toward full decarbonization. This vision is supported by both technical and operational measures.

- **Energy Efficiency Design Index (EEDI):** Introduced in 2011, the EEDI is mandatory for new ships. It sets minimum efficiency standards depending on ship type and size. This supplier-driven measure promotes innovation in hull design, propulsion, and the use of alternative energy sources (IMO, 2011).
- **Ship Energy Efficiency Management Plan (SEEMP):** Applicable to all ships, this plan requires operators to implement onboard strategies such as voyage planning, speed optimization, and better maintenance to reduce fuel use (IMO 2011, IMO 2012).
- **Energy Efficiency Existing Ship Index (EEXI):** Effective January 2023, the EEXI extends the principles of the EEDI to existing vessels. Compliance may involve engine power limits or retrofits with energy-saving devices to meet efficiency standards (IMO 2021a, IMO 2011, MEPC.335(76) 2021).
- **Carbon Intensity Indicator (CII):** Also starting in 2023, the CII gives ships an annual rating from A to E based on CO₂ emissions per transport work. Ships rated D or E for three consecutive years must submit a corrective action plan, which encourages the adoption of low-carbon technologies (IMO 2021b, IMO 2011)

Overall, these measures create strong incentives for shipowners and operators to adopt smart solutions that comply with regulations. Among the promising technologies, Wind-Assisted Ship Propulsion (WASP) systems stand out as they harness renewable wind energy to reduce fuel consumption and emissions. Additionally, shipping companies face increasing carbon fees, which enhance the economic value of energy efficiency measures, making them both environmentally and economically beneficial (European Commission, 2021). As a result, WASP technologies are gaining market momentum, with various systems offering improved efficiency, automation, and compact design, helping shipowners comply with regulations while simultaneously improving vessel performance. Overall, environmental policy, market pressure, and new technologies are driving the development of a new generation of environmentally friendly propulsion solutions.

2.1 Wind-Assisted Ship Propulsion Systems

Wind-assisted propulsion systems harness wind energy to reduce fossil fuel reliance, employing various technologies with distinct aerodynamic principles and designs. Among the most recognized are:

2.1.1 Flettner Rotors:

Cylindrical rotating devices that exploit the Magnus effect to generate lift. Among the most widely studied systems that perform well in producing additional thrust. According to Thies and Ringsberg [35], fuel savings from these systems range from 10% to 30%, depending on ship type and conditions. However, challenges arise from their high rotational speeds, large deck space requirements, and complex design. Their size and appearance also limit use on certain vessels such as passenger ships or those with low freeboard.



Figure 1: E-Ship 1 equipped with four Flettner rotors [53]

2.1.2 Kite Sails:

Large kites that generate thrust by being deployed ahead of the vessel, pulling it forward. In favourable wind conditions, they can cut fuel use by up to 35% [57]. They require only a small deck footprint and can reach stronger winds higher above the surface. However, their performance is highly dependent on sea and wind conditions. Launching and retrieving kites requires complex systems and trained crew, while limited manoeuvrability during deployment has reduced their widespread adoption.



Figure 2: Kite Sail on ship

2.1.3 Rigid Sails

Also called wing sails or hard sails, resemble airplane wings and operate as fixed aerodynamic structures. They usually function passively, producing thrust at favourable wind angles. Fuel savings are estimated to range from 20% to 30% [58]. However, their fixed geometry makes them less adaptable to variable wind conditions and installing them often requires ship modifications that can reduce flexibility.



Figure 3: Berge Olympus fitted with four Rigid sails [54]

2.1.4 Suction Sails

A system designed to enhance lift by managing airflow through boundary layer control. It integrates the aerodynamic principles of rigid sails with added adaptability. Suction-based technologies improve on passive designs by actively regulating airflow with suction. Air is drawn into the system via integrated mechanisms, which delay flow separation and boost lift. Research and experimental data suggest that these systems achieve a lift-to-drag ratio comparable to or better than Flettner rotors, while maintaining a compact and lightweight profile [32].



Figure 4: eSAIL system retrofitted in vessel Bow Olympus [56]

2.2 Review of Works for WASP Performance Assessment

The practical deployment of wind-assisted propulsion systems (WASP) has transitioned from theoretical modeling to real-world applications, with several studies demonstrating measurable fuel savings, emissions reductions, and operational feasibility. This section reviews works on various WASP systems, drawing from literature, field trials, and simulations to assess their performance [10].

Notable deployments include systems on chemical tankers and bulk carriers. For instance, a chemical tanker operated by Odfjell SE was retrofitted with suction sail units in 2023 as part of a strategy to meet IMO's EEXI and CII requirements while improving operational efficiency [11], [27], [28]. Performance modeling indicated expected fuel consumption reductions of approximately 10%, depending on wind conditions and voyage profile [32]. A later retrofit on a larger chemical tanker with additional units forecasted reductions of approximately 1,616 tonnes of CO_{2e} per year, with potential savings reaching 2,908 tonnes annually if advanced weather routing is applied. These reductions are expected to improve the vessel's CII rating, supporting regulatory compliance [32], [13].

Academic research has provided validation through modeling. A diploma thesis from the National Technical University of Athens (NTUA) by Thalassinos (2025) modeled the performance of a bulk carrier retrofitted with both Flettner rotors and suction sail units [12]. Using parametric modeling and CFD-based performance curves, the study evaluated fuel consumption across various wind scenarios. The results showed potential fuel savings of up to 44% when side forces were considered, and up to 48% when side forces were neglected [12].

Wind tunnel testing has also played a crucial role in validating aerodynamic performance across WASP systems. Collaborations with research institutions have conducted controlled experiments that confirmed CFD predictions, demonstrating that active flow control, such as suction, significantly delays flow separation, resulting in higher lift coefficients and improved thrust generation [32]. Technical reports detail aerodynamic optimization processes that led to improvements in lift-to-power ratios compared to earlier prototypes [32].

Additionally, the EU-funded WASP project, coordinated by the International Windship Association (IWSA), has compiled performance data from multiple vessels equipped with different WASP technologies [29]. The project provides comparative insights into operational profiles, integration challenges, and fuel savings across systems, supporting the conclusion that various WASP approaches offer a balance of efficiency, automation, and retrofit potential [29].

Together, these studies and trials confirm that WASP systems are viable for reducing fuel use and emissions. Their modular designs, automated operations, and aerodynamic efficiencies make them suitable for a range of vessel types and operating conditions. The consistent performance across simulations, field trials, and wind tunnel tests highlights their role in the transition toward low-carbon shipping.

2.3 Suction-Based Sail System – eSAIL

Suction-based sail systems represent a significant category of wind-assisted propulsion (WASP) technologies, designed to enhance thrust generation while minimizing drag through advanced aerodynamic principles. Inspired by early concepts such as the Cousteau Foundation’s TurboVoile project, these systems utilize a porous surface and internal fans to regulate airflow around the sail structure [33]. By actively controlling the boundary layer, suction sails maintain stable aerodynamic performance across a range of wind conditions, making them a versatile option for reducing fuel consumption in maritime applications.

The primary advantage of suction-based sails lies in their ability to combine the aerodynamic efficiency of rigid sails with dynamic adaptability to varying environmental conditions. Unlike passive systems, they employ active airflow control, which enhances lift and reduces drag, contributing to improved propulsion efficiency. This section explores the basic working principles of suction-based sail systems and their potential for integration into modern shipping, supported by theoretical and empirical studies.

Following figure illustrates a typical suction sail system, showcasing its compact and streamlined design, which is well-suited for retrofitting on various vessel types. The system’s structure, with its thick foil profile and internal ventilation, enables precise control of airflow, a key factor in its aerodynamic performance.



Figure 5: Suction sail example [32]

2.3.1 Basic Working Principles

Suction wings are wing sails equipped with a mechanical air suction mechanism and a notably thick profile. The core mechanism involves boundary layer suction, where ventilators installed inside the sail profile draw air through a porous surface. This process controls airflow around the sail's "thick" foil shape, accelerating it at the leading edge, or the "nose" of the egg-shaped cross section. This acceleration creates a region of low pressure along the suction side and the top-left side of the profile, significantly reducing the drag coefficient while maintaining a high lift coefficient—up to 7–8, depending on the angle of attack and suction efficiency [28].

When the sail is inactive, drag is created due to its presence in incoming wind as shown below.

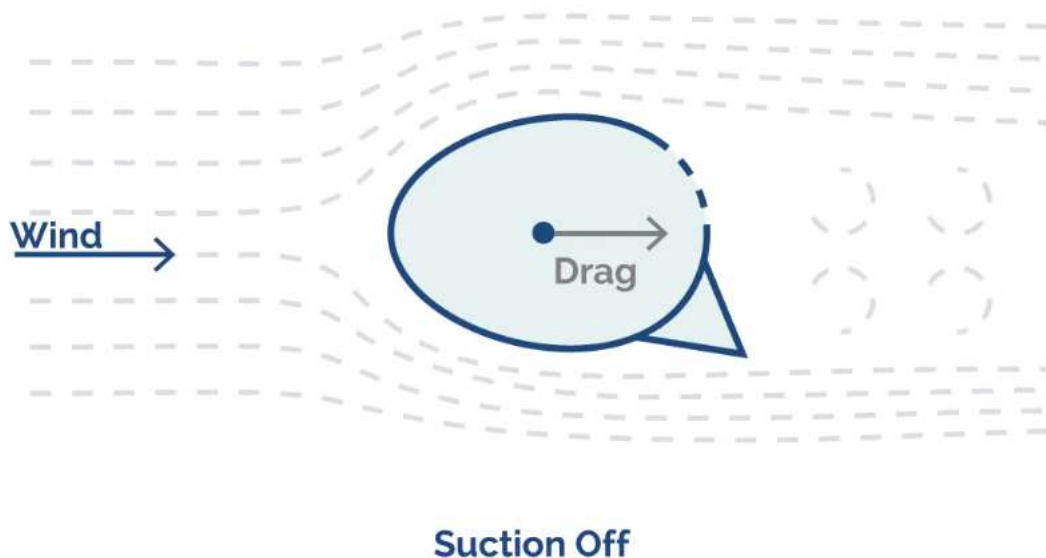


Figure 6: Suction sail inactive [32]

Upon activation, the suction mechanism generates lift while substantially reducing drag, enhancing the sail's contribution to propulsion.

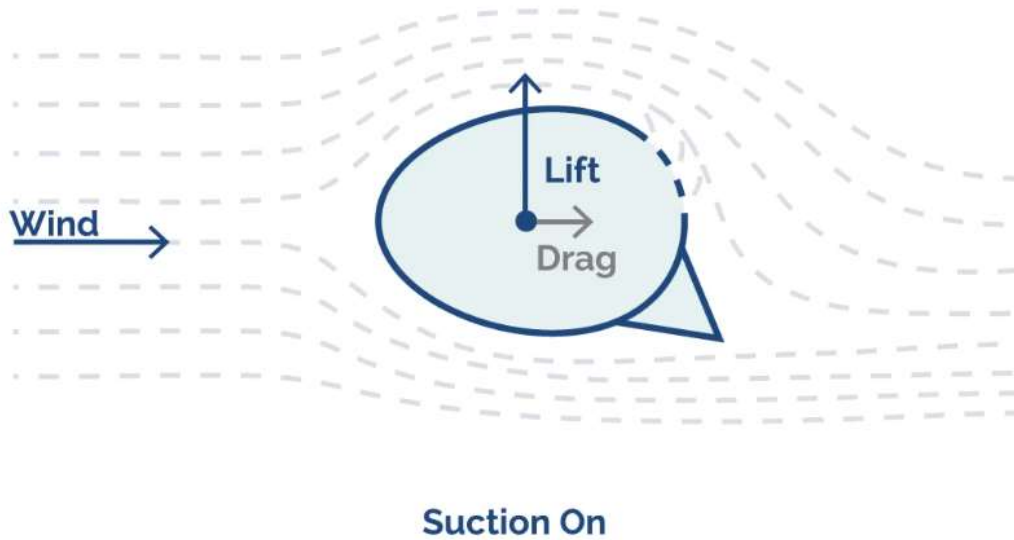


Figure 7: Suction sail active [32]

With appropriate rotation the lift can be further increased while minimal increase in drag is induced.

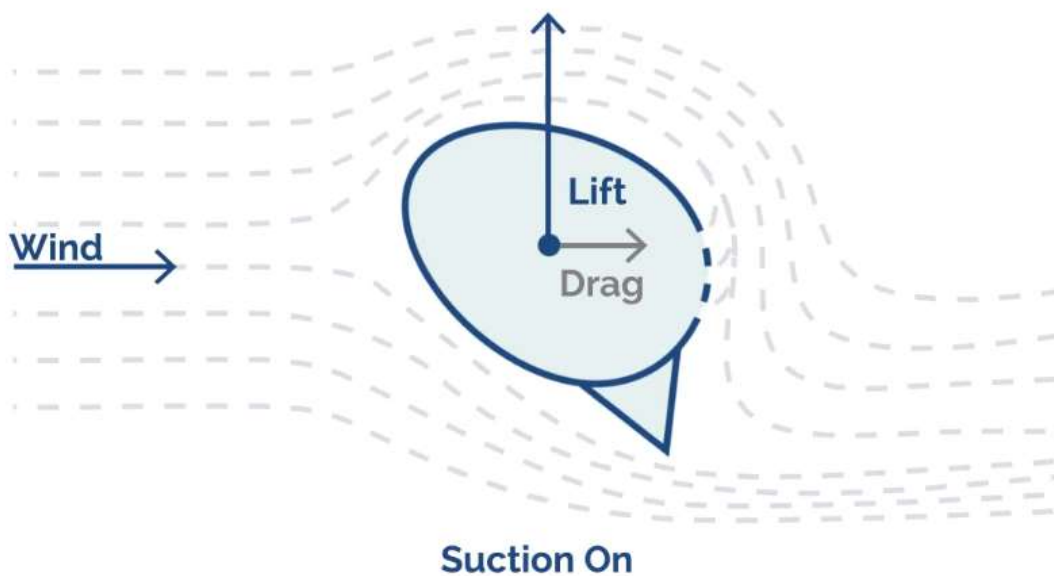


Figure 8: Suction sail active with appropriate rotation [32]

2.3.2 Performance Analysis and Application

The performance of suction-based sail systems has been evaluated through advanced analytical methods and practical applications. Computational Fluid Dynamics (CFD) simulations have been employed to optimize sail geometry, fan characteristics, and suction porosity, with wind tunnel tests validating a lift-to-power ratio improvement of approximately 20% compared to earlier prototypes [32]. These systems achieve lift coefficients comparable to other WASP technologies, such as Flettner rotors, but with lighter, more compact structures and lower energy requirements [32]. Automated sensors and actuators adjust suction levels and sail orientation in real time, enhancing efficiency across diverse wind conditions [32].

From a physics perspective, the boundary layer control mechanism delays flow separation, reducing stall risks and enabling higher efficiency in variable winds [33]. The design prioritizes mechanical simplicity, minimizing maintenance needs and enhancing reliability for integration on both new builds and retrofitted vessels [32].

2.3.3 Application in Thesis Modeling

In this thesis, a suction-based sail system was selected as a case study to demonstrate the application of a general mathematical model for WASP technologies, using data available for the eSAIL system developed by bound4blue [32]. The model, implemented in MATLAB, evaluates interactions between ship resistance, propulsion efficiency, and fuel consumption under various wind scenarios to quantify potential benefits [12], [19], [20], [23]. This approach ensures the framework's applicability to other WASP systems, with the suction sail serving as a practical example due to accessible performance data.

Chapter 3: Theoretical Model and Methodology

This chapter presents the mathematical model and methodology developed to evaluate ship propulsion performance with and without wind-assisted technologies. Following the literature review and regulatory framework discussed in Chapter 2, the focus here is on the technical approach, including the key equations for resistance, propulsion, and fuel consumption. A flowchart is provided to illustrate the computational sequence, ensuring a structured and reproducible framework. The specific application scenarios are deferred to Chapter 4, where they are implemented and analyzed.

3.1 Methodology Overview

The methodology integrates hydrodynamic, aerodynamic, and propulsion principles into a computational framework implemented in MATLAB. It begins with input data on the vessel's particulars, environmental conditions (such as wind speed, direction, and wave parameters), and optional wind-assisted system specifications. Resistance components are calculated step-by-step, followed by propeller and engine performance evaluations, leading to fuel consumption estimates.

The computational sequence is summarized in the following flowchart, which outlines the main steps:

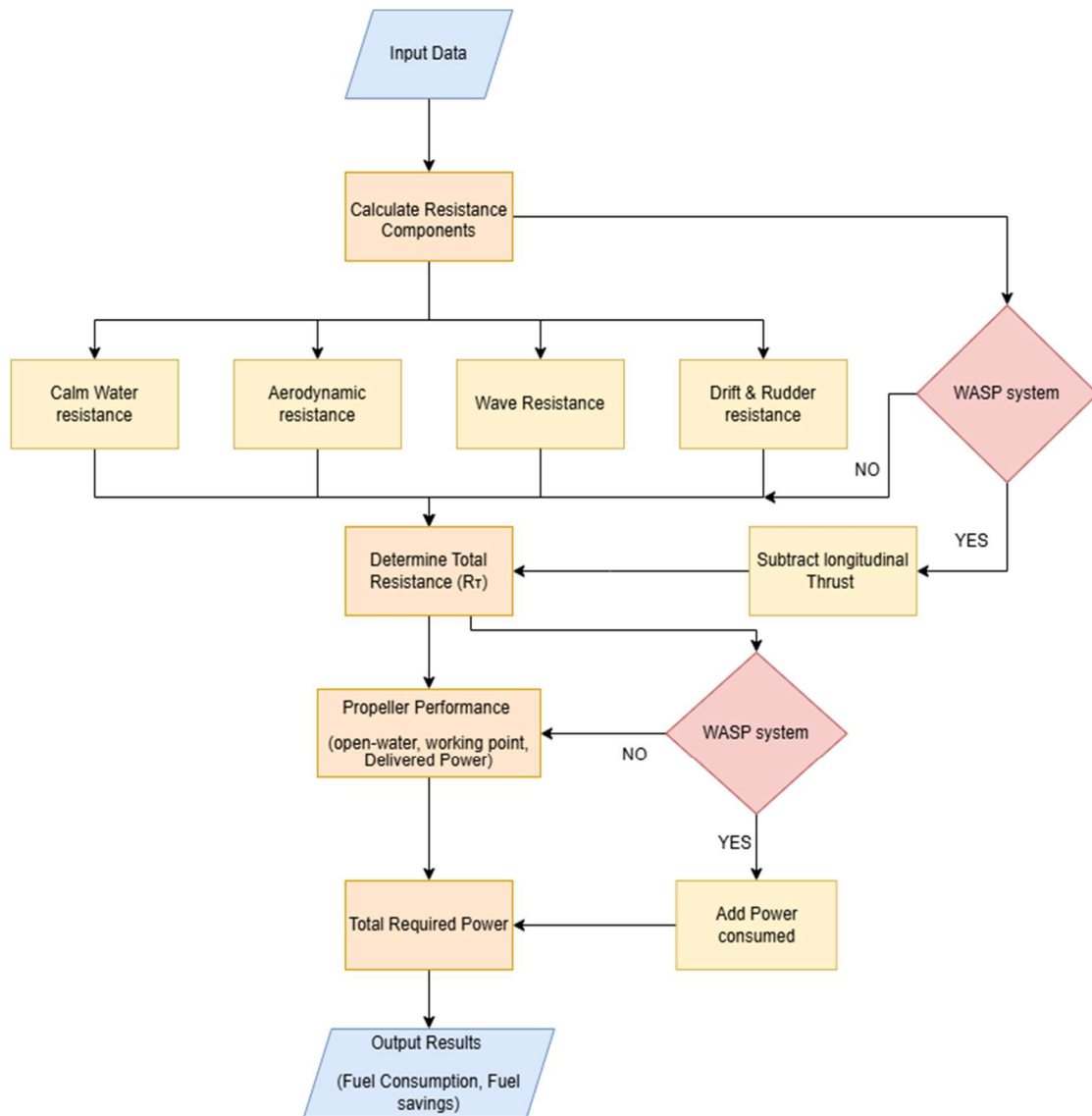


Figure 9: Methodology Flowchart

3.2 Components of Ship Resistance

The total resistance acting on a vessel can be expressed as the sum of hydrodynamic and aerodynamic contributions, corrected by the thrust generated by the wind-assisted system (when installed) [45], [46], [47].

The general formulation used in this thesis is:

$$R_T = R_{cw} + R_{AA} + R_{AW} + R_{drift} + R_{rudder} - F_{sail} \quad (3.1)$$

Where:

- R_{cw} : Calm-water resistance,
- R_{AA} : Added aerodynamic resistance due to wind,
- R_{AW} : Added resistance in waves,
- R_{drift} : Resistance due to drift forces from sideslip,
- R_{rudder} : Resistance from rudder deflection,
- F_{sail} : Longitudinal thrust contribution of the wind-assisted system (when installed).

Data for each component has been individually treated using empirical or semi-empirical methods, ensuring the final formulation is consistent with the case study vessel and the data provided. The next subsections will provide the detailed theoretical treatment of each term [45], [46], [47].

3.2.1 Calm-Water Resistance (R_{cw})

Calm-water resistance represents the baseline hydrodynamic drag experienced by a ship's hull when moving through still water, serving as the foundational component for assessing overall propulsion performance. It primarily arises from frictional effects due to the viscous interaction between the hull and surrounding fluid [40]. This resistance can be estimated through various methods, including model tank tests for empirical validation, computational fluid dynamics (CFD) simulations for detailed flow analysis, and semi-empirical formulas based on regression of experimental data, such as those from the International Towing Tank Conference (ITTC) standards [45], [46], [47].

3.2.2 Added aerodynamic resistance due to wind

Wind blowing against the hull and superstructure which is above waterline creates aerodynamic resistance. This resistance is computed by following equation:

$$R_{AA} = \frac{1}{2} \cdot \rho_A \cdot C_{DA} \cdot (\psi_a) \cdot A_{XV} \cdot U_a^2 - \frac{1}{2} \cdot \rho_A \cdot C_{DA}(0) \cdot A_{XV} \cdot V_s^2 \quad (3.2)$$

Where:

A_{XV} : area of maximum transverse section exposed to wind [m^2]

C_{DA} : wind resistance coefficient

V_s : measured ship's speed [m/s]

U_a : apparent wind speed [m/s] at reference height

ρ_A : mass density of air [kg/m^3]

ψ_a : apparent wind direction at reference height (0 means heading wind)

For specific true wind speed U_t and true wind angle ψ (where $\psi = B_{WT} - \text{Heading}$, see Figure 11) the apparent wind speed, U_a and apparent wind angle, ψ_a can be calculated from the equations:

$$U_a = \sqrt{U_t^2 + V_s^2 - 2 \cdot U_t \cdot V_s \cdot \cos(180 - \psi)} \quad (3.3)$$

$$\psi_a = \tan^{-1} \left(\frac{U_a^2 + V_s^2 - U_t^2}{2 \cdot U_a \cdot V_s} \right) \quad (3.4)$$

3.2.3 Added resistance in waves

3.2.3.1 Added Resistance in Regular Waves

The effect of waves on ship resistance is quantified by the added resistance in waves (R_{AW}), which accounts for additional drag from wave reflection, diffraction, and ship motions. Following Liu & Papanikolaou (2008), the added resistance in regular waves is calculated by:

$$R_{AW} = R_{AWR} + R_{AWM} \quad (3.5)$$

Where:

R_{AWR} : reflection/diffraction component,

R_{AWM} : mean drift force component,

Refer to Appendix B: Added resistances, B.1.2 Added wave resistance.

3.2.3.2 Added Resistance in Irregular Waves

In real seas, the energy of waves is distributed across a range of frequencies. To capture this, the regular-wave results are integrated over a wave spectrum. A JONSWAP spectrum is used in this work, parameterized by the significant wave height H_s and spectral peak period T_p . The spectral density function $S(\omega)$ assigns relative weight to each wave frequency [47].

The added resistance in irregular waves is therefore:

$$\bar{R}_{aw} = 2 \int_0^{\infty} S(\omega) \cdot \frac{R_{aw}(\omega)}{\zeta_{\alpha}^2} \cdot d\omega \quad (3.6)$$

Where:

S : spectrum function [m^2/Hz]

ω : angular velocity [rad/s]

ζ_{α} : wave amplitude [m]

This integral is computed numerically for each heading angle. The spectral density function is:

$$S(H_s, T_p, \gamma) = \alpha^* \cdot H_s^2 \cdot \omega_p^{-5} \cdot \omega^{-5} \cdot \exp \left[-\frac{5}{4} \left(\frac{\omega}{\omega_p} \right)^{-4} \right] \cdot \gamma \exp \left(\frac{(\omega - \omega_p)^2}{2\sigma^2 - v_p^2} \right) \quad (3.7)$$

With parameters:

H_s : significant wave height [m],

T_p : spectral peak period [s],

ω_p : peak angular frequency [rad/s],

γ : peak shape factor,

σ : spectral width

α^* : scaling factor depending on γ

3.2.4 Drift & Rudder Resistance

When exposed to side winds, the ship develops a drift angle β , to balance the lateral aerodynamic force. The hull generates a hydrodynamic restoring side force and yaw moment, while the rudder must deflect to maintain course. Both the hull and the rudder introduce additional drag components that contribute to the vessel's total resistance. To estimate velocity and construct a ship with a sailing system, it is crucial to account for significant rudder angles and the induced resistance caused by drift.

- Drift resistance $X_D(\beta)$, empirically expressed as a polynomial in the drift angle.
- Rudder resistance F_{NX} , proportional to the rudder normal force and its deflection angle δ .

The following diagram depicts the drift angle and rudder deflection resulting from the combined influence of aerodynamic and hydrodynamic moments acting on the ship, which is fitted with a Wind Propulsion System (WPS).

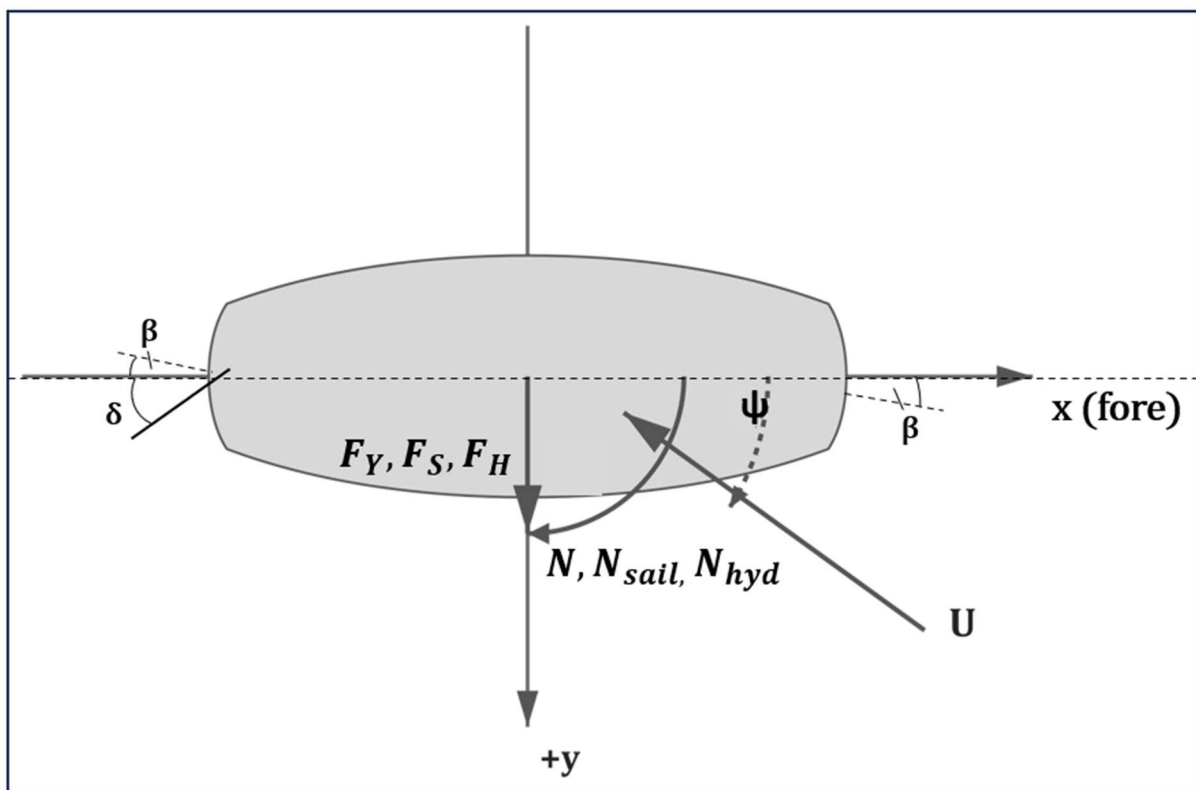


Figure 12: System of coordinates

As illustrated in coordinate system (Fig. 12), the y direction is positive to starboard and the x-direction is positive in the forward ship direction.

The drift and rudder forces are obtained using Skogman (1985) and Inoue et al. (1981) formulations, with aerodynamic inputs from Fujiwara's coefficients. The balance of lateral forces and yaw moments is solved for each wind angle, producing the values of $\beta(\psi)$ and $\delta(\psi)$.

The formulations are based on the equilibrium of moments that can be formed, under steady-state conditions, around the center of gravity, which is located at the midship section for simplicity.

The aerodynamic moment N , the sails' moment N_{sail} , and the hydrodynamic moment N_{hyd} , are all in balance when:

$$N + N_{\text{sail}} + N_{\text{hyd}} = 0 \quad (3.8)$$

The yaw moment N_H and the rudder-induced moment N_R make up the hydrodynamic moment N_{hyd} .

The formula for N_{sail} (moment by the sails) is as follows:

$$N_{\text{sail}} = F_S \cdot x_S \quad (3.9)$$

x_S : the horizontal lever arm of the sail force to midship

F_S : Sail Lateral force

The aerodynamic lateral force and yaw moment are given by:

$$F_Y(\psi) = -C_Y(\psi) \cdot \frac{1}{2} \rho_A U_A^2 A_{YV} \quad (3.10)$$

$$N(\psi) = -C_N(\psi) \cdot \frac{1}{2} \rho_A U_A^2 A_{YV} L_{OA} \quad (3.11)$$

Where:

ρ_A : is the air density,

A_{YV} : is the lateral projected area above the waterline,

Loa: is the overall ship length,

$C_Y(\psi)$ and $C_N(\psi)$ are the Fujiwara aerodynamic coefficients, dependent on wind angle ψ .

U_A : is the apparent wind speed calculated based on equation (3.28)

In the present work, the aerodynamic coefficients $C_Y(\psi)$ and $C_N(\psi)$ were evaluated using the semiempirical regression method of Fujiwara [41], which provides explicit angle-dependent expressions. The coefficients were calculated as functions of the wind incidence angle ψ , making the aerodynamic loads vessel specific and angle-sensitive.

The methodology for calculating these coefficients, as well as their contribution to the resistance formulation, is presented in appendix (B.1.2).

The negative sign on $F_Y(\psi)$ and $N(\psi)$ reflects the difference in coordinate system conventions:

- In Fujiwara's framework [41], the wind is assumed to act from the port side, leading to a positive definition opposite the convention adopted here.
- In this thesis, which is based on Elger (2019) [40] and Skogman (1985) [39], that form the basis of the present drift and rudder balance model, the wind is assumed to act from the starboard side, as shown in Figure 12.

To ensure consistency between aerodynamic forces and the hydrodynamic/yaw equilibrium equations, a negative sign was applied in Eqs. (3.10) and (3.11) above.

In the next step, an auxiliary factor is computed using x_R as the lever arm from the rudder's pressure point to midship:

$$Y_{m0} = \frac{1}{0.5 \cdot \rho \cdot T \cdot L_{WL} \cdot V_S^2} \cdot \left(F_Y + F_S - \frac{1}{x_R} \cdot (N + N_{\text{sail}}) \right) \quad (3.12)$$

The underwater portion of the hull's effective aspect ratio, or AR_h , is:

$$AR_h = \frac{2 \cdot T}{L_{WL}} \quad (3.13)$$

The lateral force's hydrodynamic derivatives, Y'_v and Y''_v , are as follows:

$$Y'_v = -0.5 \cdot \pi \cdot AR_h - 1.4 \cdot C_B \cdot \frac{B_{WL}}{L_{WL}} \quad (3.14)$$

$$Y''_v = -6.6 \cdot (1 - C_B) \cdot \frac{T}{B_{WL}} + 0.08 \quad (3.15)$$

Drift dimensionless speed v' is calculated:

$$v' = \frac{\left(Y'_v + \frac{AR_h \cdot L_{WL}}{x_R} \right) + \sqrt{\left(Y'_v + \frac{AR_h \cdot L_{WL}}{x_R} \right)^2 + 4 \cdot Y'_{vv} \cdot Y_{m0}}}{Y'_{vv}} \quad (3.16)$$

Drift angle β is:

$$\beta = \arcsin v' \quad (3.17)$$

y -direction ship velocity is:

$$v = v' \cdot V_S \quad (3.18)$$

x -direction ship velocity is:

$$u = \sqrt{V_S^2 - v^2} \quad (3.19)$$

The drift-related non-dimensionalized additional resistance is:

$$c_{XD} = 0.0833 \cdot \beta - 0.1 \cdot \beta^2 + 0.0041667 \cdot \beta^3 \quad (3.20)$$

Drift-related additional resistance is then:

$$X_D = c_{XD} \cdot 0.5 \cdot \rho \cdot u^2 \cdot L_{WL} \cdot T \cdot 10^{-3} \quad (3.21)$$

Yaw moment by the hull is:

$$N_H = 0.5 \cdot \rho \cdot L_{WL}^2 \cdot T \cdot V_s^2 \cdot (-AR_h \cdot v') \quad (3.22)$$

The span x_3 across the rudder area A_r and mean chord line c_{mean} are used to compute the effective aspect ratio, or AR_r , before calculating the rudder angle:

$$AR_r = 2 \cdot AR_{\text{geometric}} = 2 \cdot \frac{x_3}{c_{\text{mean}}} \quad (3.23)$$

The wake decreases the inflow speed v_r to the rudder:

$$v_r = V_s \cdot (1 - w) \quad (3.24)$$

In the beginning, the lateral rudder force F_{NY} needs to be calculated using an arbitrary inflow angle α_r , such as -5° :

$$F_{NY} = 0.5 \cdot \rho \cdot \frac{6.13 \cdot AR_r}{2.25 + AR_r} \cdot A_r \cdot v_r^2 \cdot \sin(\alpha_r) \quad (3.25)$$

The term "hydrodynamic force" refers to the force that the rudder action exerts on the ship's hull. Using regression analysis based on model testing α_H , which is the ratio of the force on the hull caused by the rudder to the rudder force, is calculated [33]:

$$\alpha_H = 0.64 \cdot C_B - 0.154 \quad (3.26)$$

To find the rudder angle δ , the following formula is used:

$$\delta = 0.5 \cdot \arcsin \left(\frac{2}{-(1+\alpha_H) \cdot x_R \cdot \frac{F_{NY}}{\sin(\alpha_r)}} \cdot (0.5 \cdot \rho \cdot AR_h \cdot L_{WL}^2 \cdot T \cdot V_s^2 \cdot v' - N - N_{\text{sail}}) \right) \quad (3.27)$$

The rudder force F_{NY} needs to be calculated again using the new inflow angle. The rudder's additional resistance is:

$$F_{NX} = -F_{NY} \cdot \sin \delta \quad (3.28)$$

Finally, rudder moment is:

$$N_R = -(1 + \alpha_H) \cdot x_R \cdot F_{NY} \cdot \cos \delta \quad (3.29)$$

The total resistance from Side Forces can now be estimated by adding Drift Resistance and Rudder's additional resistance:

$$R_{drift} + R_{rudder} = X_D + F_{NX} \quad (3.30)$$

3.2.5 WASP thrust contribution

When WASP units are installed, they produce a net longitudinal effective thrust that reduces the required propeller thrust. Their performance could be either estimated by analytical expressions, semi-empirical methods or directly provided as an experimental dataset from the manufacturer, where longitudinal thrust, perpendicular force, and (if applicable) power consumption are tabulated, as functions of apparent wind speed and angle.

The net contribution to resistance is $-F_{sail}$, while the perpendicular force component is included to the lateral balance equations, modifying rudder and drift resistance.

3.3 Propeller and Engine Performance

3.3.1 Propeller Open Water Performance and Working Point

The propeller open-water characteristics are an essential element in linking the resistance model with the propulsion and fuel consumption calculations. The thrust generated by the propeller depends on its advance ratio and efficiency, which in turn are affected by modifications in total resistance and required effective power due to wind-assisted propulsion [1], [40].

The propeller performance is described through the standard open-water coefficients:

$$T_0 = \frac{R_T}{1 - t} \quad (3.31)$$

Where:

- T_0 is the open-water thrust [N],
- R_T is the total ship resistance [N],
- t is the thrust deduction factor (a dimensionless coefficient accounting for the reduction in thrust due to hull interaction).

$$V_0 = (1 - w) \cdot V \quad (3.32)$$

Where:

- V_0 is the advance speed of the propeller [m/s],
- w is the wake fraction (a dimensionless factor representing the velocity reduction behind the hull),
- V is the ship speed [m/s].
-

Constant number:

$$C = \frac{k_T}{J^2} = \frac{\frac{T_0}{\rho \cdot n_0^2 \cdot D^4}}{\left(\frac{V_0}{n_0 \cdot D}\right)^2} = \frac{T_0}{\rho \cdot V_0^2 \cdot D^2} \quad (3.33)$$

is utilized to create following curve:

$$k_T = c \cdot J^2 \quad (3.34)$$

The previous curve is plotted in the same diagram with the $k_T = f(J)$ (3.34) curve of the propeller (from open water performance results) and the intersection of these two provides the working point of ship propeller system. Using the propeller advance coefficient J at this intersection, the open-water propeller speed n_0 , efficiency η_0 , and torque Q_0 are estimated.

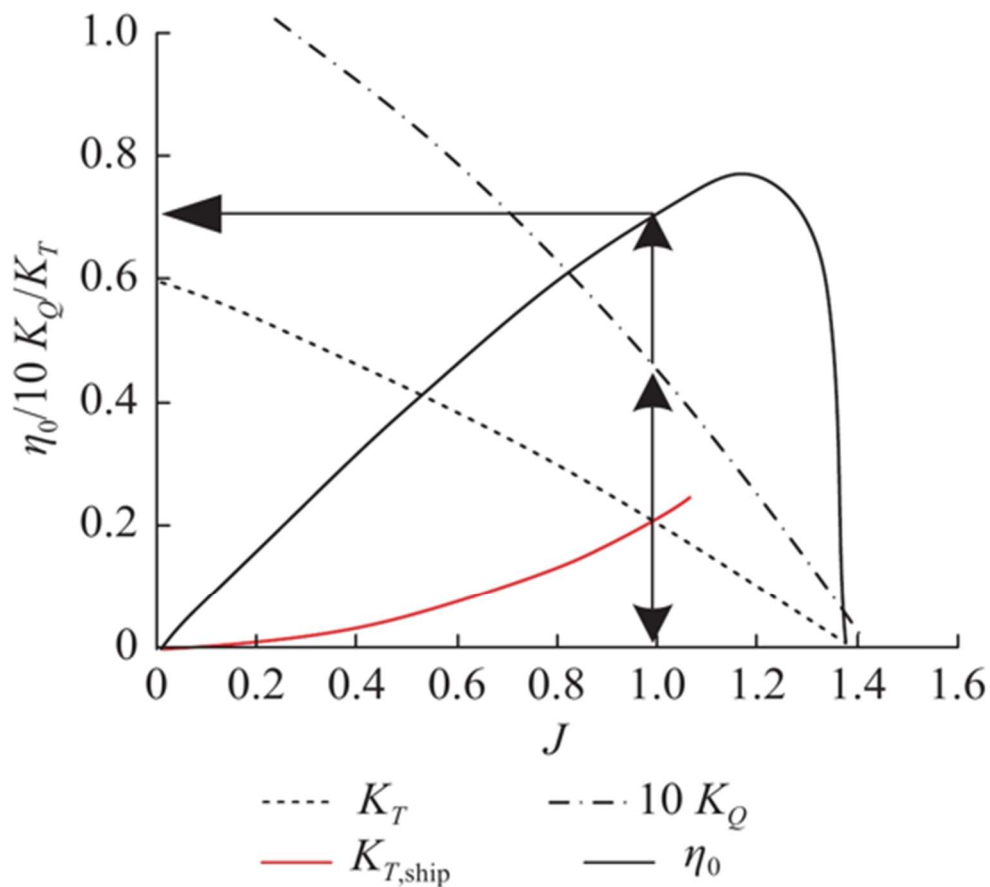


Figure 13: Intersection of hull demand thrust coefficient curve and propeller open water performance curve for an example vessel [59]]

$$n_0 = \frac{V_0}{J \cdot D} \quad (3.35)$$

$$\eta_0 = f(J) \quad (3.36)$$

$$Q_0 = \frac{T_0 \cdot V_0}{2 \cdot \pi \cdot n_0 \cdot \eta_0} \quad (3.37)$$

3.3.2 Delivered Power and Main Engine Load

To account for hull-propeller interactions and performance adjustments, the final shaft speed n , delivered torque Q_d , and delivered power P_d are calculated as follows, based on the open-water values corrected by the RPM correction factor C_n , rotative efficiency η_R , and power correction factor C_p :

$$n = C_n \cdot n_0 \quad (3.38)$$

$$Q_d = \frac{Q_0}{\eta_R} \quad (3.39)$$

$$P_d = C_p \cdot 2 \cdot \pi \cdot n \cdot Q_d \quad (3.40)$$

The engine load is calculated relative to the Maximum Continuous Rating (MCR) of the main engine:

$$\text{Load}(\%) = 100 \cdot \frac{P_d}{MCR} \quad (3.41)$$

3.3.3 Wind-Assisted Power Integration

When wind-assisted devices are in operation, in addition to the delivered power required for propulsion, the wind-assisted system introduces an auxiliary power demand. Each unit requires a certain consumption P_{con} to maintain the flow control used for thrust generation [13], representing the suction fan consumption of each unit. For a configuration with N units, the total consumption is:

$$P_{WASP} = P_{con} \cdot N \quad (3.42)$$

This power requirement is added to the delivered power to obtain the total required power, which represents the combined load from the main engine and the power for the wind-assisted system supplied by auxiliary sources:

$$P_{req} = P_d + P_{WASP} \quad (3.43)$$

3.4 Fuel Consumption Model

The estimation of fuel consumption is based on the relationship between the delivered power and the engine's specific fuel oil consumption (SFOC). This model converts the delivered power into fuel mass flow and allows the assessment of operational performance with and without the contribution of the wind-assisted system [14].

The fuel consumption rate for the main engine is given by:

$$m_{\text{fuel,baseline}} = P_d \cdot \text{SFOC} \quad (3.44)$$

Where:

$m_{\text{fuel,baseline}}$ is the fuel consumption rate [kg/h],

P_d is the delivered power [kW],

SFOC is the specific fuel oil consumption for the main engine [g/kWh].

The SFOC is typically provided by the engine manufacturer and depends on the load fraction relative to MCR. For simplicity, it can be considered constant or interpolated from the engine load-SFOC curve.

Since wind-assisted systems are installed, additional electrical consumption is provided by auxiliary generators. The fuel consumption for this auxiliary load is calculated separately using the auxiliary engine's specific fuel oil consumption (SFOC_{AE}):

$$m_{\text{fuel,WASP}} = P_{\text{WASP}} \cdot \text{SFOC}_{\text{AE}} \quad (3.45)$$

The total fuel consumption is then:

$$m_{\text{fuel,total}} = m_{\text{fuel,baseline}} + m_{\text{fuel,WASP}} \quad (3.46)$$

This formulation accounts for the propulsion demand plus the parasitic load of the system, providing a comprehensive estimate of the vessel's fuel usage.

Chapter 4: Case Study

4.1 Ship's Particulars

In this section, the main particulars of the case study vessel are presented. These data are necessary as input for the resistance calculations that follow.

Table 1: Principal Particulars of Ship

PRINCIPAL PARTICULARS	
LENGTH O.A.	229 m
LENGTH B.P.	225.5 m
BREADTH (MLD.)	32.26 m
DEPTH (MLD.)	20.05 m
DESIGNED DRAFT	12.20 m
C_B @ DESIGNED DRAFT	0.8624
DEADWEIGHT (DESIGNED DRAFT)	64911.79 t
SCANTLING DRAFT	14.45 m
C_B @ SCANTLING DRAFT	0.8772
DEADWEIGHT (SCANTLING DRAFT)	80996.09 t
LIGHTSHIP WEIGHT	13800.11 t
MAIN ENGINE	MAN B&W 6S60ME-C8.5-TII
TRANSMISSION EFFICIENCY η_s	0.99
P_{MCR}	9930 kW
$P_{MCR_ME,lim}$	8230 kW
n_{MCR}	90.4 rpm
TYPE OF FUEL (ME & AE)	DIESEL/GAS OIL

4.2 eSAIL Description and Data Source

The eSAIL is a suction-assisted rigid sail developed by bound4blue, representing a modern wind-assisted propulsion (WASP) technology. It is available in three models (Models 1, 2, and 3), each with distinct dimensions and power ratings. Following consultation with the manufacturer, Model 2 was selected as the optimal choice for the case study vessel.

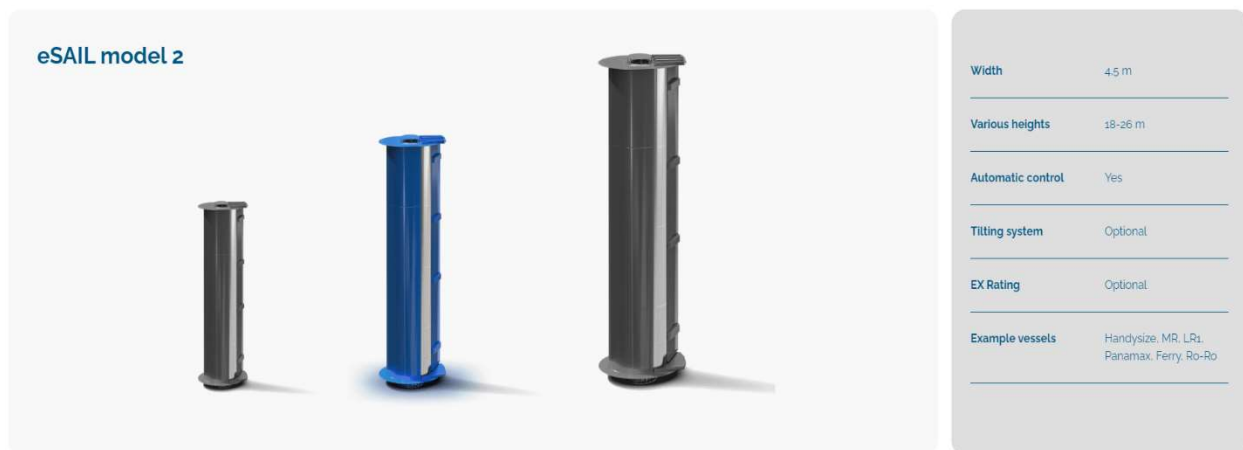


Figure 14: eSAIL model 2

For this analysis, four eSAIL units were adopted, each measuring 23 m in height and 4.5 m in width, installed on deck. This configuration adds a total of 414 m² to the vessel's exposed lateral area. Originally, the ship's lateral area above waterline was 2024.5 m², and with the addition of the four eSAIL units, it increases to 2438.5 m². This enhanced lateral area directly impacts the aerodynamic components of Total Resistance and is accounted for in the calculation of aerodynamic coefficients with the FUJIWARA method.

The positioning of the four eSAIL units on the main deck is shown in Figure 4.2. They were arranged symmetrically along the deck to minimize interference effects and to ensure effective distribution of aerodynamic forces.

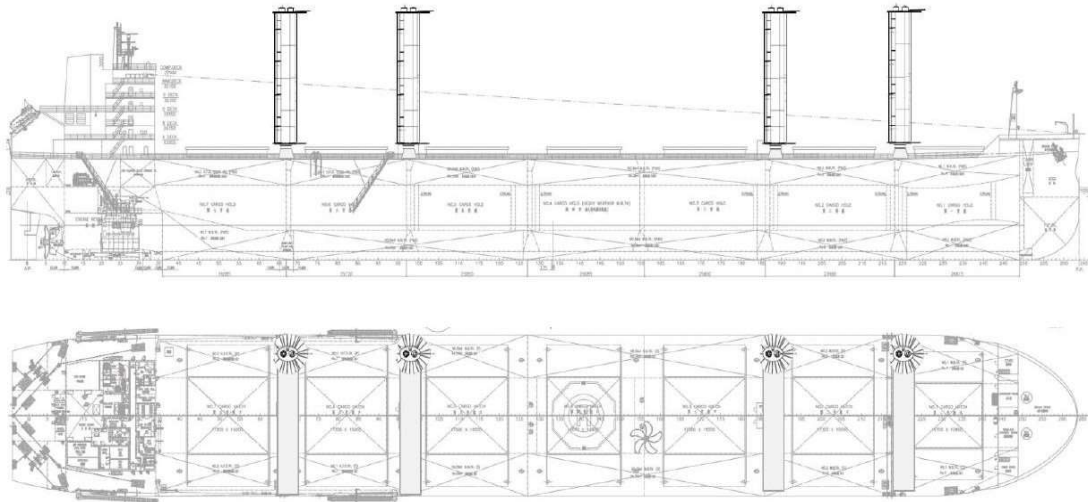


Figure 15: Position of eSAIL units on the ship's main deck

The performance data per eSAIL unit were provided by the manufacturer, and include:

- Longitudinal force (DF): effective thrust component (positive when assisting propulsion).
- Perpendicular force (HF): side force generated perpendicular to the ship's centerline.
- Power consumption (P_{con}): electrical power required for the suction fans and control systems.

These values were tabulated as functions of the apparent wind speed (U_a) and apparent wind angle ($\psi\alpha$).

The control logic of the system ensures that:

- When thrust is positive, the eSAIL operates normally, consuming auxiliary power (P_{con}).
- When thrust is negative (unfavorable wind condition), the system is automatically deactivated, avoiding unnecessary energy consumption.

The following figures present the manufacturer-provided eSAIL performance data for the case study vessel at a service speed of $V_s = 11 \text{ kn}$ and a true wind speed of $U_t = 10 \text{ m/s}$. The plots show the variation of Longitudinal thrust (DF), Perpendicular force (HF), and power consumption (P_{con}) as functions of wind angle.

To better illustrate the performance of the eSAIL under different wind conditions, the data were interpolated across varying apparent wind scenarios to reveal how both the force components and power demand evolve with changing wind direction and intensity.

1. Variable Apparent Wind Speed (U_a)

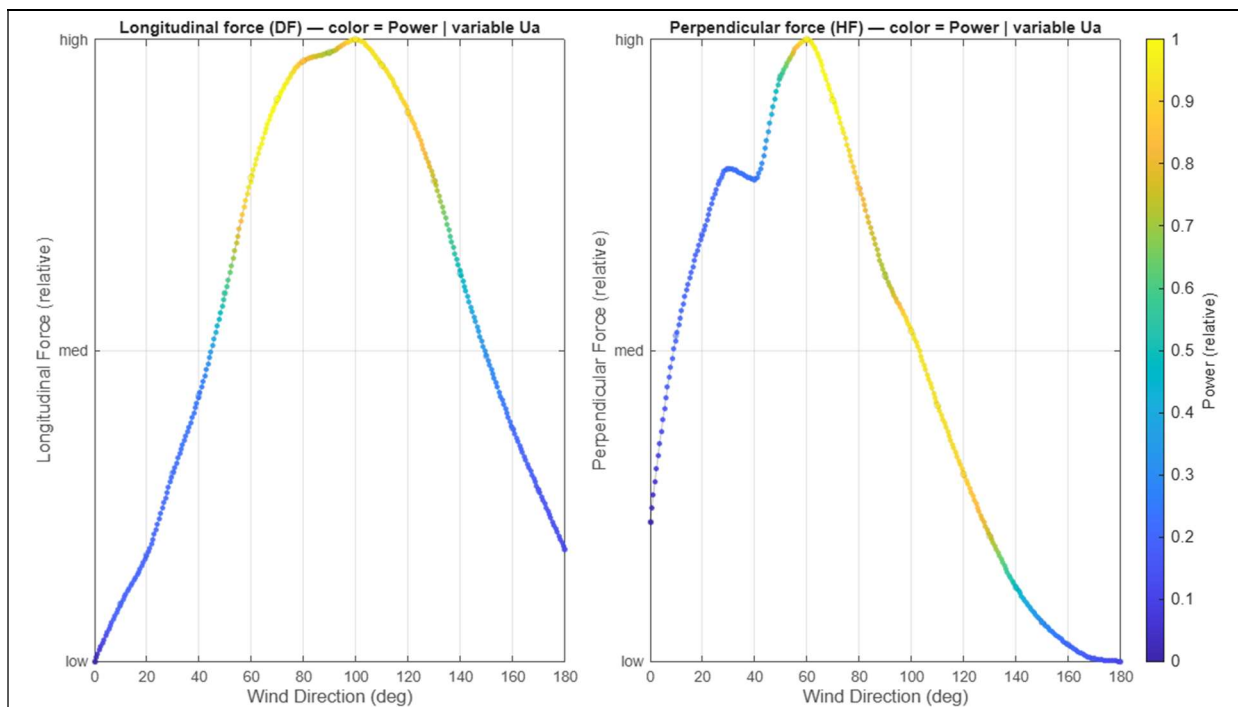


Figure 16: Relative variation of eSAIL effective Forces and Power Consumption under Variable Apparent Wind Speed

2. Constant Apparent Wind Speed (U_a)

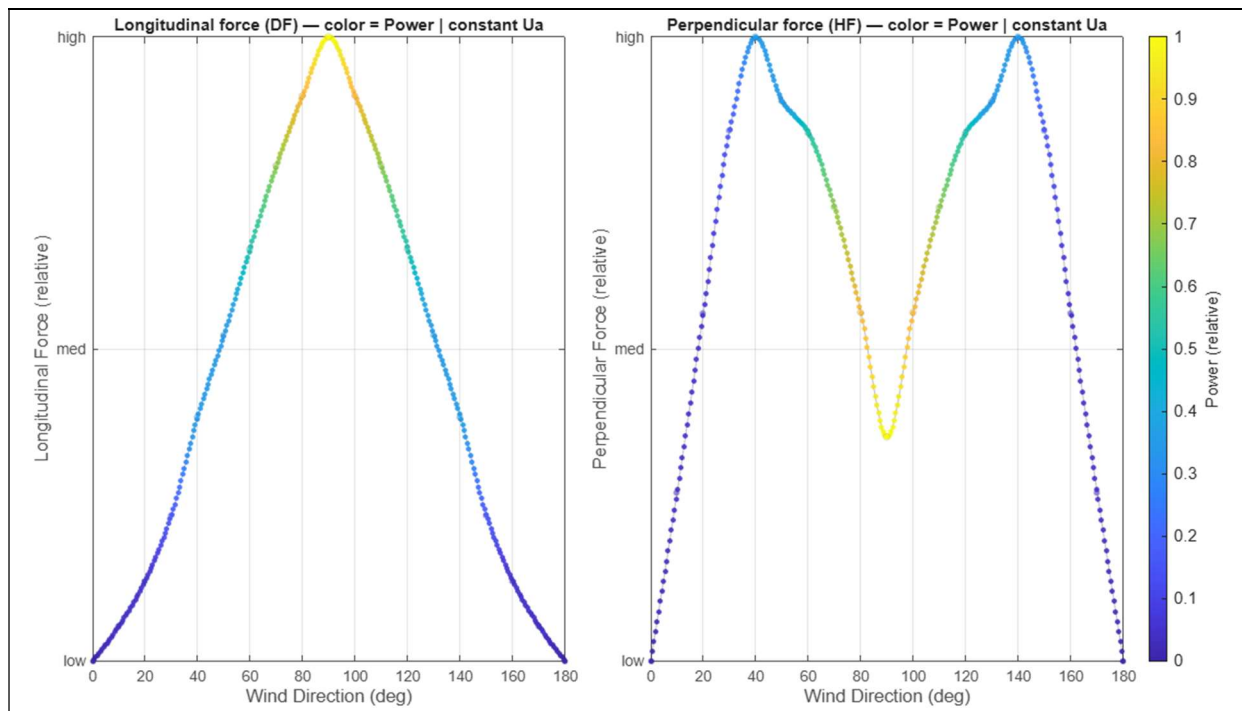


Figure 17: Relative variation of eSAIL effective Forces and Power Consumption under Constant Apparent Wind Speed

4.2.1 Defined Scenarios

To evaluate the impact of the eSAIL® system, four scenarios were defined, combining the presence or absence of sails with two different treatments of wind speed:

Scenario 1: Conventional ship without eSAIL, with variable apparent wind speed.

Scenario 2: Conventional ship without eSAIL, with constant apparent wind speed ($U_a = 10$ m/s).

Scenario 3: Ship equipped with four eSAIL units, with variable apparent wind speed.

Scenario 4: Ship equipped with four eSAIL units, with constant apparent wind speed ($U_a = 10$ m/s).

In the constant-wind cases (Scenarios 2 and 4), the apparent wind speed is fixed at 10 m/s for all headings, providing a simplified baseline for comparison.

4.3 Resistance Components

In this section, the methodology for calculating the main resistance components of the vessel is presented. Each contribution is examined separately, starting from calm water resistance, followed by wind resistance and wave resistance. The results provide the basis for the total resistance formulation used in the subsequent analysis [49].

4.3.1 Resistance from Model Tests

The resistance of the case study vessel in calm water and in Scantling draft was derived from data obtained through Towing tank Model Test results, as documented in the available Model Test report [49]. These results are visually represented in the following diagram.

For this analysis, the vessel is assumed to operate at a service speed of 11 knots.

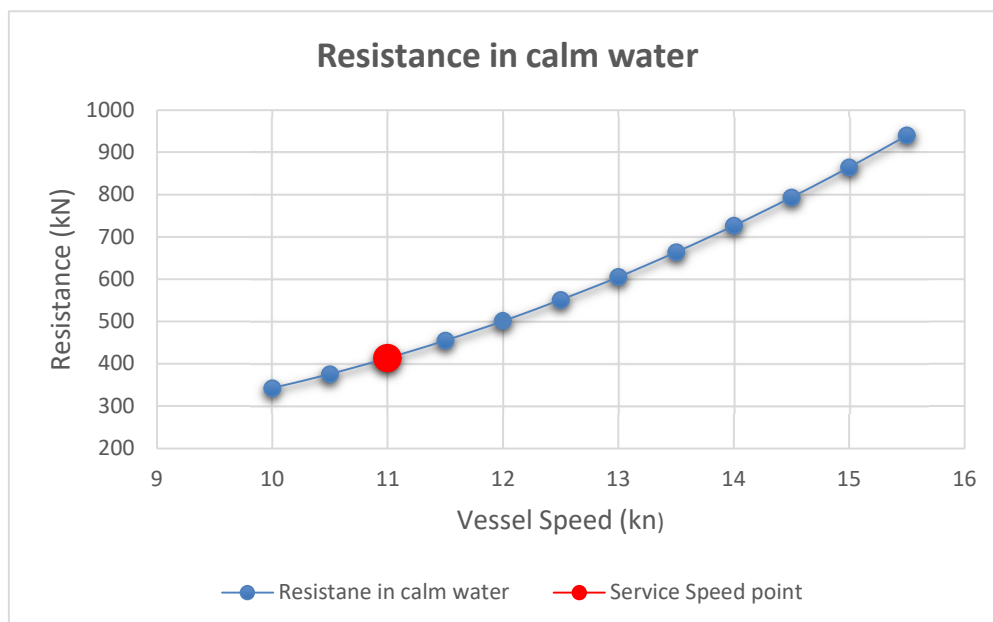


Figure 18: Resistance in calm water for Scantling draft [49]

4.3.2 Added Wind Resistance

The added aerodynamic resistance is determined from the wind resistance coefficients (C_{DA}), which vary with the wind angle of attack and these coefficients are incorporated into the mathematical calculation (Equation 3.2) to derive the final aerodynamic contribution.

The required data for computing these coefficients are provided in the following table for both the baseline vessel and the case where it is fitted with eSAIL units. In the latter scenario, the presence of the units on the deck results in notable shifts in parameters, significantly affecting the aerodynamic behavior.

Table 2: Required data in Scantling draft

Required Data			
	Baseline vessel	Fitted with eSAIL	
Loa	229	229	m
B	32.26	32.26	m
Aod	705	1119	m ²
Axv	637	637	m ²
Ayv	2024.5	2438.5	m ²
Cmc	-10.54	-7.48	m
Hbr	26.5	26.5	m
Hc	5.48	7.45	m
μ	10	10	deg

The respective plots of wind resistance coefficient versus the wind angle are depicted in the figures:

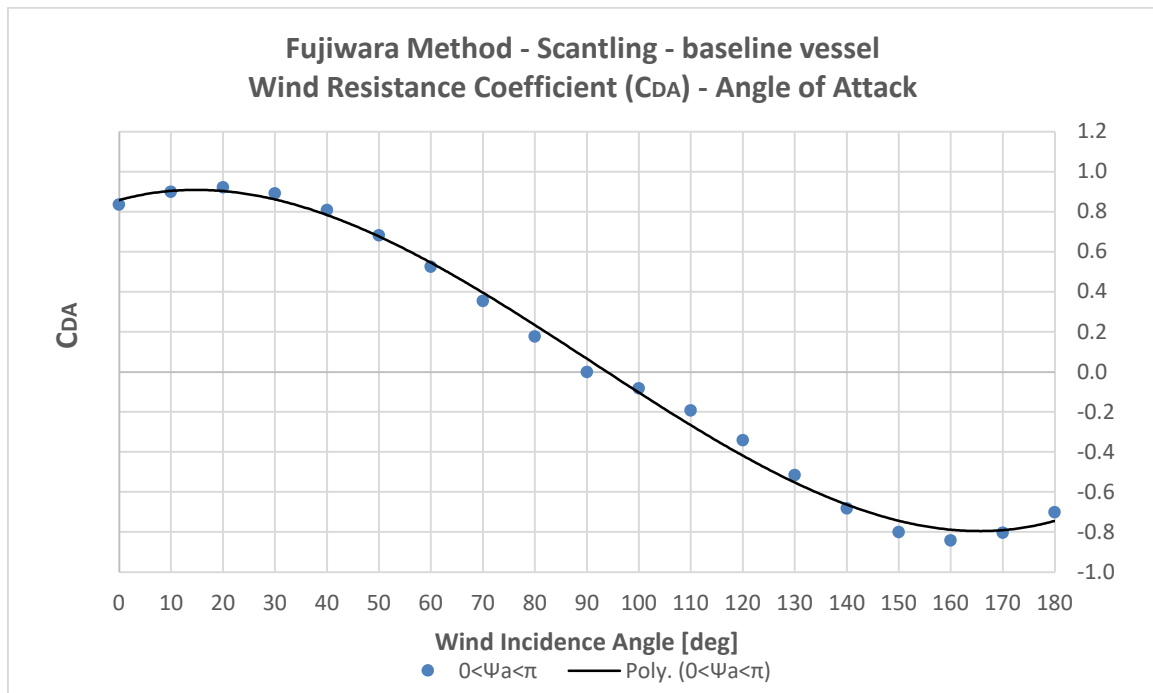


Figure 19: Wind Resistance Coefficient C_{DA} versus Wind Incidence Angle - Baseline Vessel

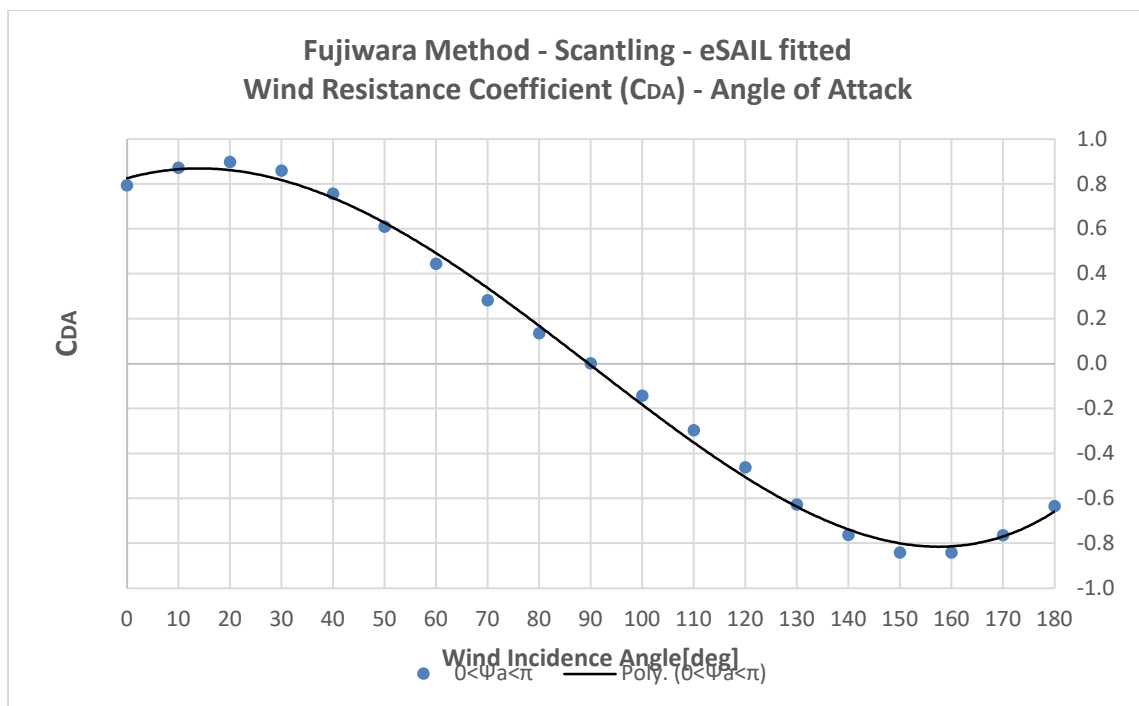


Figure 20: Wind Resistance Coefficient C_{DA} versus Wind Incidence Angle - eSAIL Fitted Vessel

The variation of the apparent wind speed (U_a) with wind direction is presented, in order to provide context for the following analysis of the case study vessel. According to Equation (3.3), U_a depends on the true wind speed (U_t), the ship's speed (V_s), and the true wind angle.

The following figure shows this variation, together with a reference case of constant $U_a = 10$ m/s. The apparent wind speed reaches its maximum when the wind acts from ahead and decreases progressively toward the stern, influencing the aerodynamic forces and the resulting hydrodynamic responses.

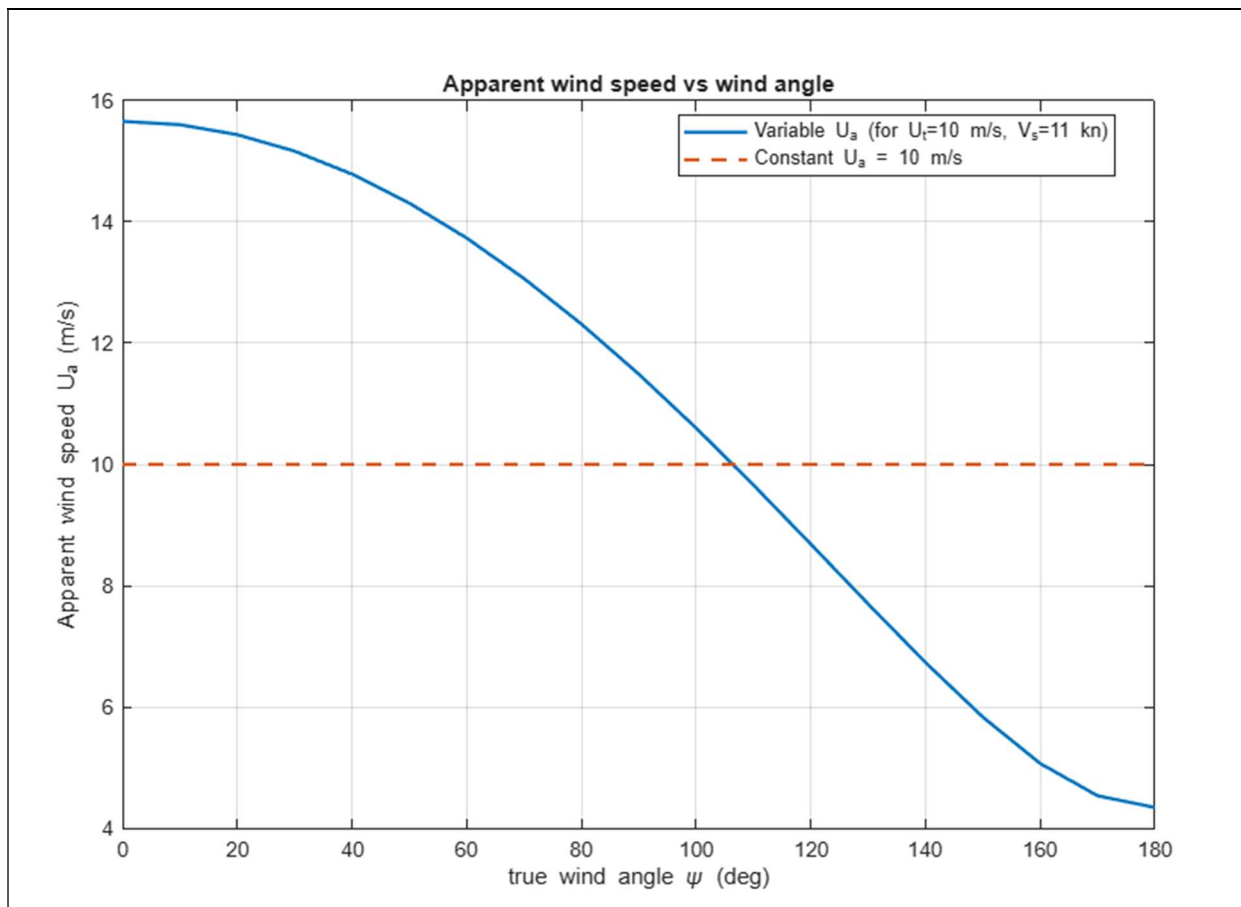


Figure 21: Apparent Wind Speed versus Wind Direction for Variable and Constant (U_a) Scenarios.

The aerodynamic Lateral Force and Yaw Moment, which contribute to vessel’s estimated side forces (Rudder & Drift resistance) will be calculated based on coefficients $C_Y(\psi)$ and $C_N(\psi)$ of Fujiwara [41]. The required data for the calculation of coefficients are the same as in Table xx.

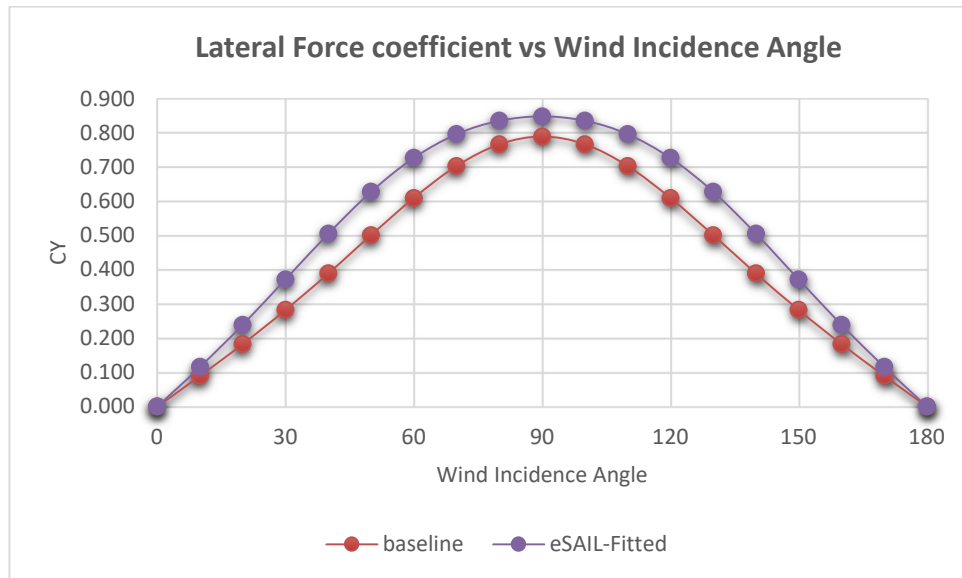


Figure 22: Lateral Force coefficient (C_Y) versus Wind Incidence Angle

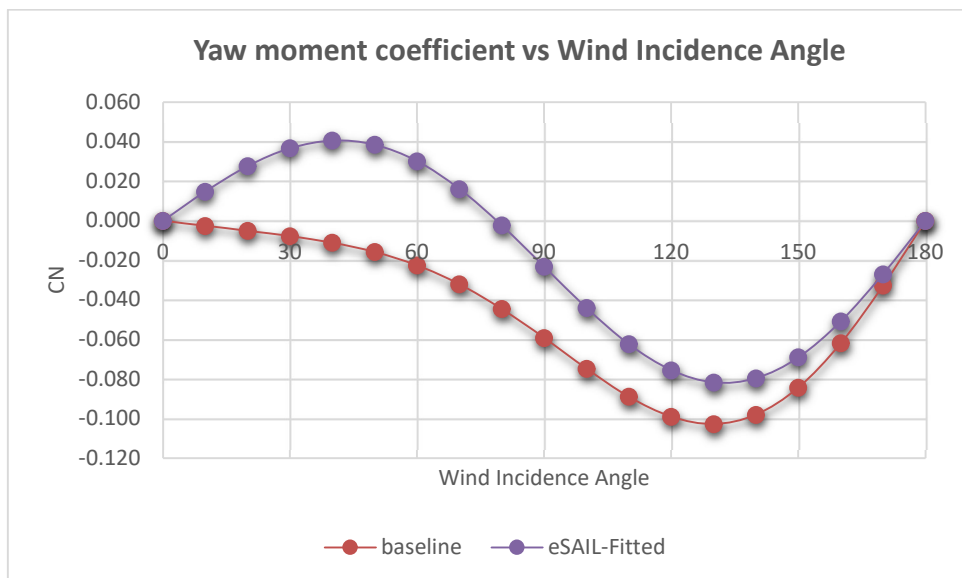


Figure 23: Yaw Moment coefficient (C_N) versus Wind Incidence Angle

4.3.3 Wave Resistance Calculation

Using MATLAB code developed for the theory of added wave resistance described in Methodology section, the added wave resistance R_{aw} (at Scantling draft) is computed versus the heading angle, where 0° (deg) is considered for bow waves.

The basic inputs for the calculation at scantling condition are provided in the table below and apply in both scenarios (baseline vessel / eSAIL-fitted)

Table 3: Parameters for calculation of wave resistance

LBP	225.5	[m]
Ta	14.45	[m]
Tf	14.45	[m]
LE1	32	[m]
LR	30	[m]
g	9.81	[m/s ²]
kyy	0.25	[-]
E1	26.75	[deg]
E2	28.27	[deg]

The significant wave height H_s is calculated, based on true wind speed ($U_t = 10$ m/s in this analysis) utilizing the following relation [60, eq. 11]:

$$H_s = 0.115 \cdot U_t^{1.41} \quad (4.1)$$

where:

$U_t = 10$ m/s.

The results are integrated over the JOHNSWAP spectrum to obtain the irregular wave resistance. This is repeated for a range of peak periods; the maximum value across T_p is taken as the conservative estimate:

$$R_{AW,max} = \max \bar{R}_{AW}(\alpha, T_p) \quad (4.2)$$

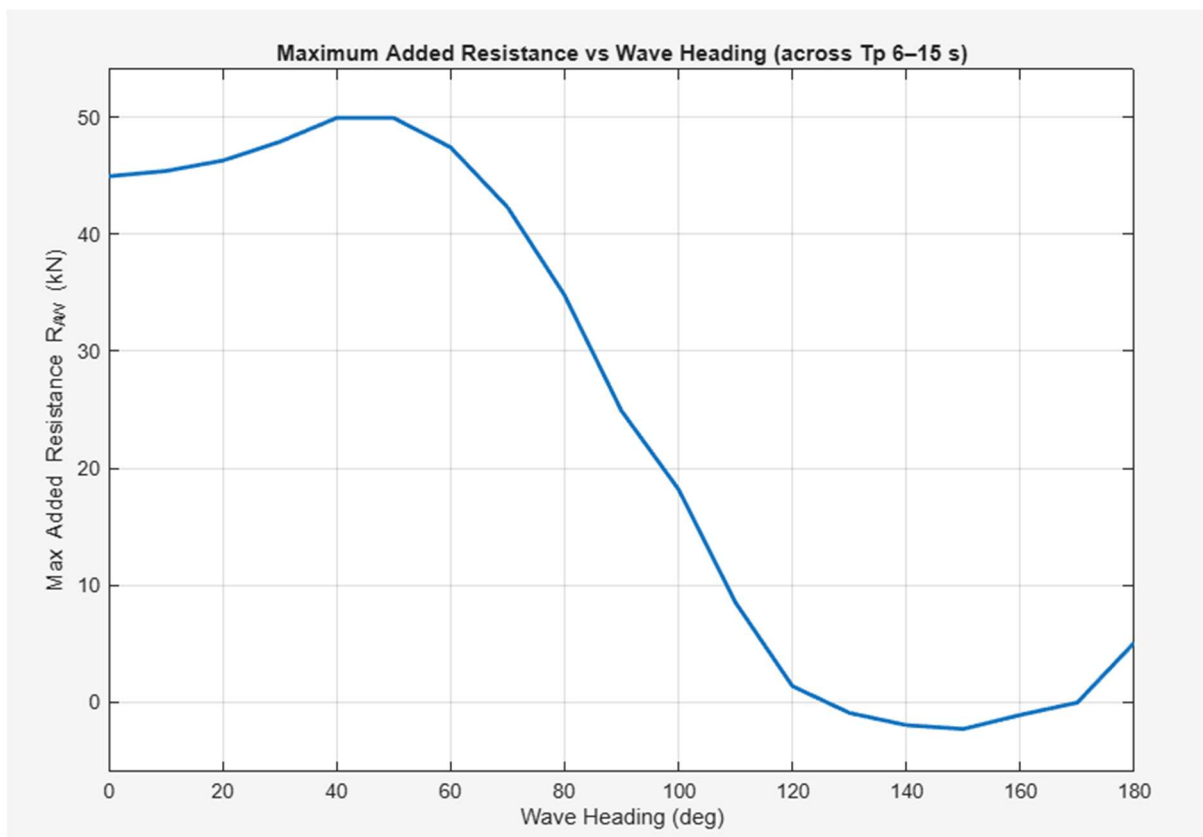


Figure 24: Max. Added Resistance in Waves across Peak Period Range ($T_p = 6-15$ s)

4.3.4. Drift & Rudder resistance

The equations presented in Section 3.2.4 were applied in MATLAB to compute the resulting drift angle, rudder angle, and their associated resistances. The results are presented together for the baseline vessel and the eSAIL-fitted vessel, enabling direct comparison.

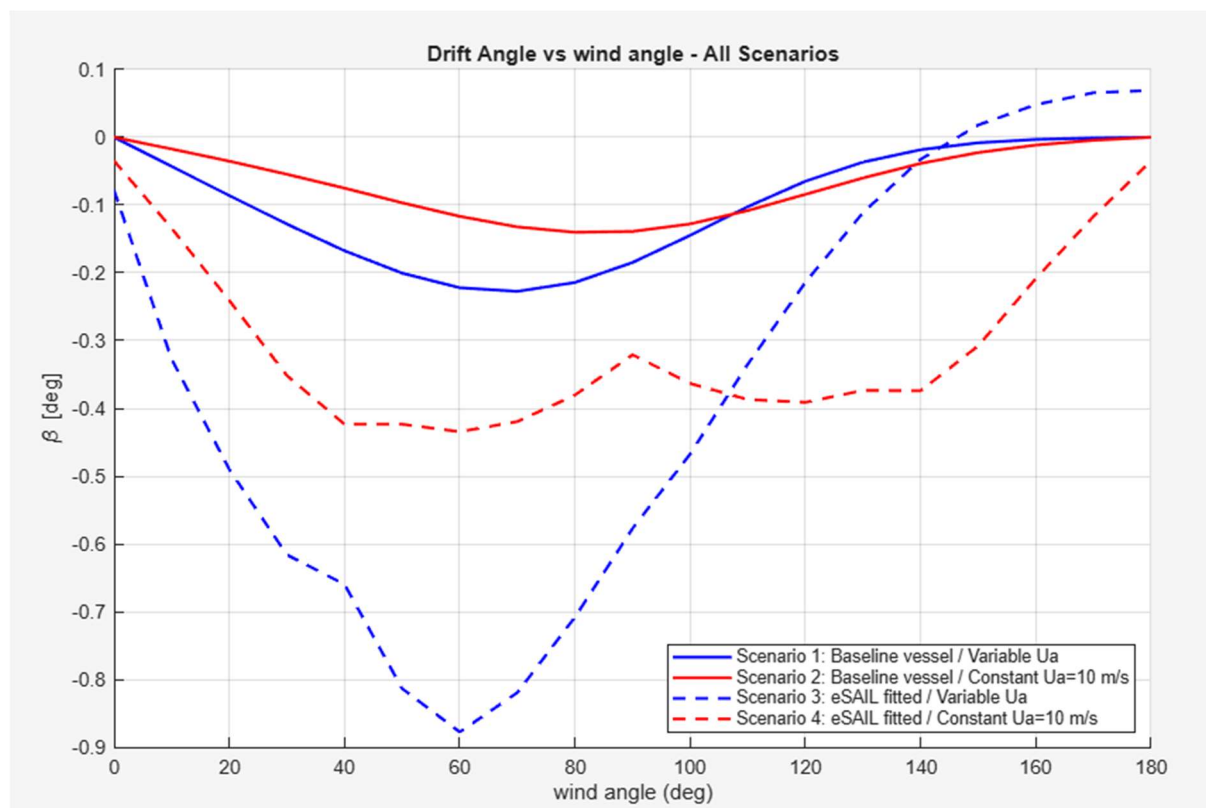


Figure 25: Variation of Drift Angle with Wind Direction under Different Apparent Wind Conditions for Baseline and eSAIL-Fitted Vessel

For all scenarios, the drift angle reaches its highest absolute values between 40° and 100° , where crosswind effects are strongest. The eSAIL-fitted case under variable apparent wind shows increased drift angles, particularly around 60° , consistent with the peak of the perpendicular effective force generated by the eSAILs, as shown in Figure 4.3. The scenarios with constant apparent wind exhibit a more symmetrical distribution of drift angles across the 0° – 180° range, reflecting the simplified nature of the fixed-wind assumption.

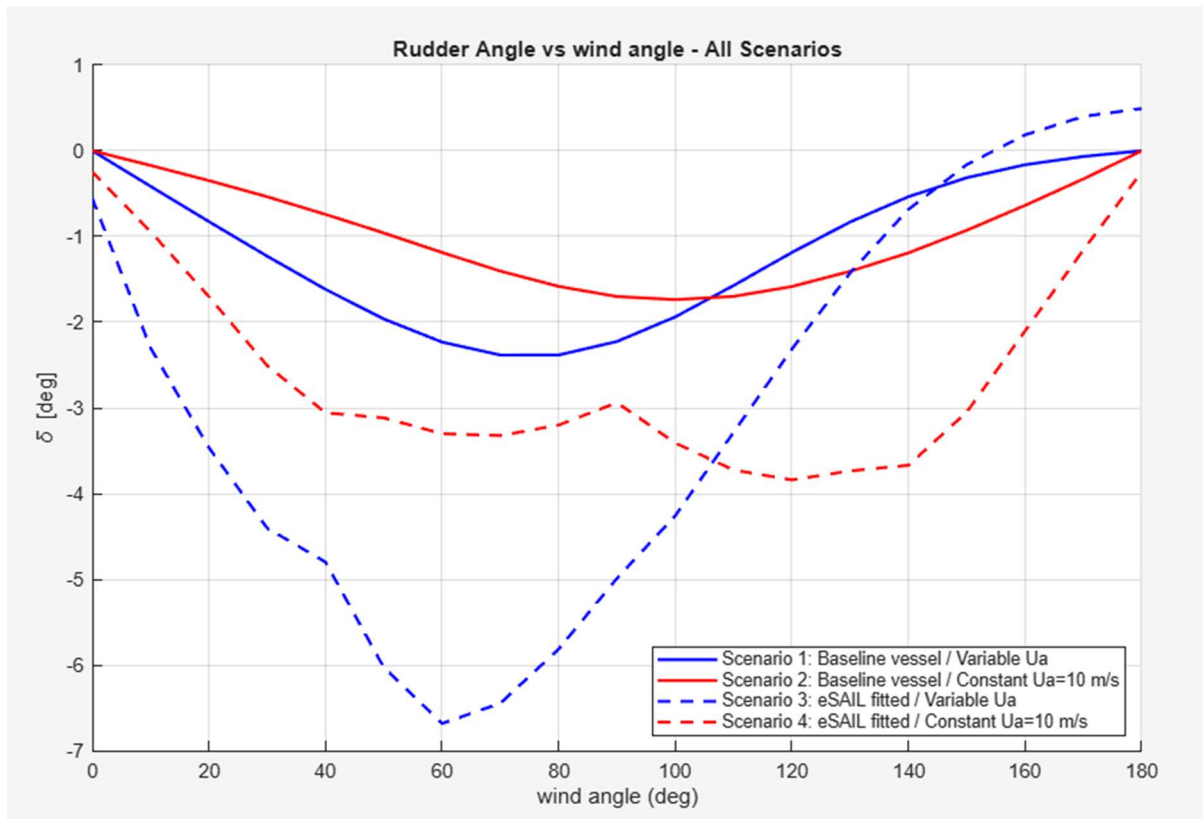


Figure 26: Variation of Rudder Angle with Wind Direction under Different Apparent Wind Conditions for Baseline and eSAIL-Fitted Vessel

The diagram shows the rudder deflection angle required to keep the vessel on a steady heading for different wind incidence angles (0° – 180°). The deflection follows the general trend of the drift angle, reaching its maximum around beam winds. The eSAIL-fitted vessel requires greater correction to maintain course stability, reflecting the higher moments introduced by the addition of the sails. In contrast to the drift angle, the rudder deflection decreases more gradually after its peak, indicating a more sustained corrective response across wider heading angles.

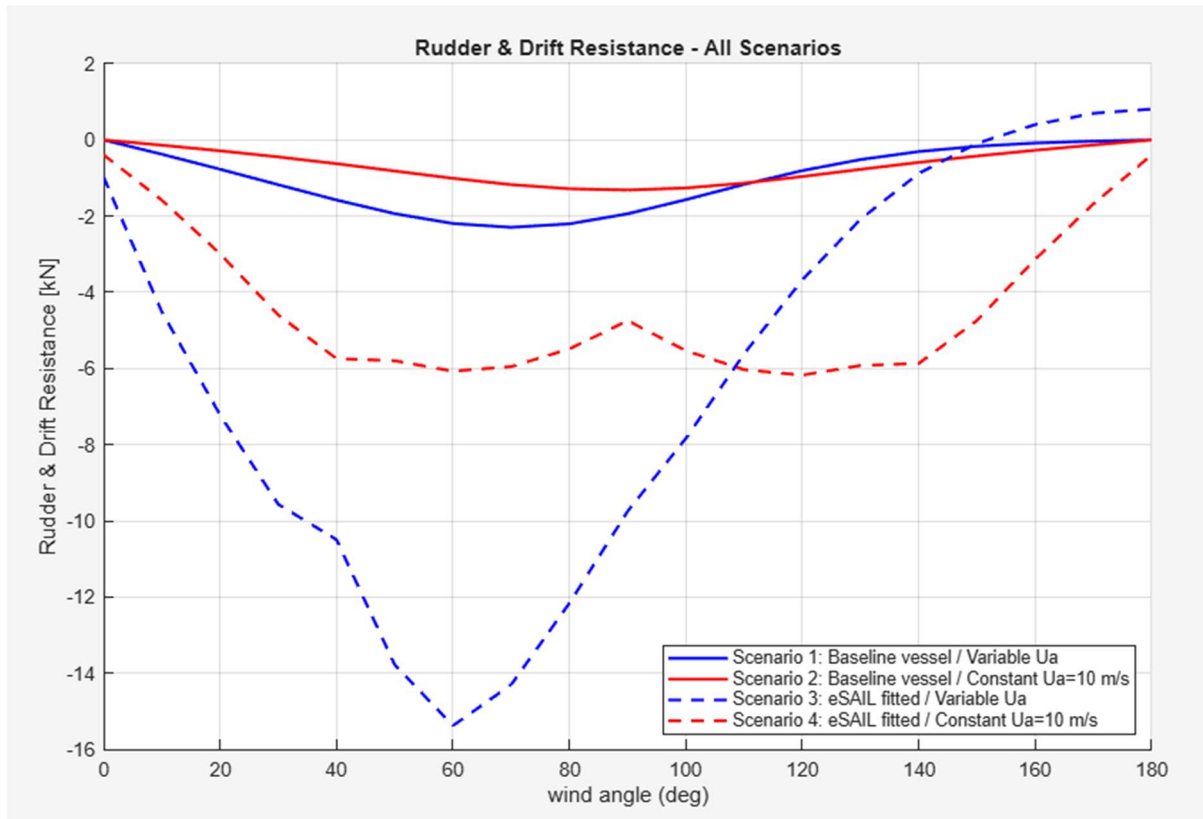


Figure 27: Rudder and Drift Resistance versus Wind Direction under Different Apparent Wind Conditions for Baseline and eSAIL-Fitted Vessel

The combined side forces from drift and rudder deflection show a clear increase when the eSAIL system is active, indicating the additional drag induced by the control forces required to maintain course. The variable apparent wind case produces the highest resistance values around 60° – 80° , aligning with the most effective operating range of the sails. The constant-wind cases display smoother variations, indicating a more uniform balance between aerodynamic and hydrodynamic effects across the examined heading range.

4.4 Total Resistance for Defined Scenarios

The total resistance on the vessel was performed by considering all hydrodynamic and aerodynamic contributions. The formulation applied follows the structure introduced in Chapter 3, where individual resistance components are defined and subsequently combined.

The sub-components along with the R_{total} are displayed in the figures below for each scenario.

Scenario 1:

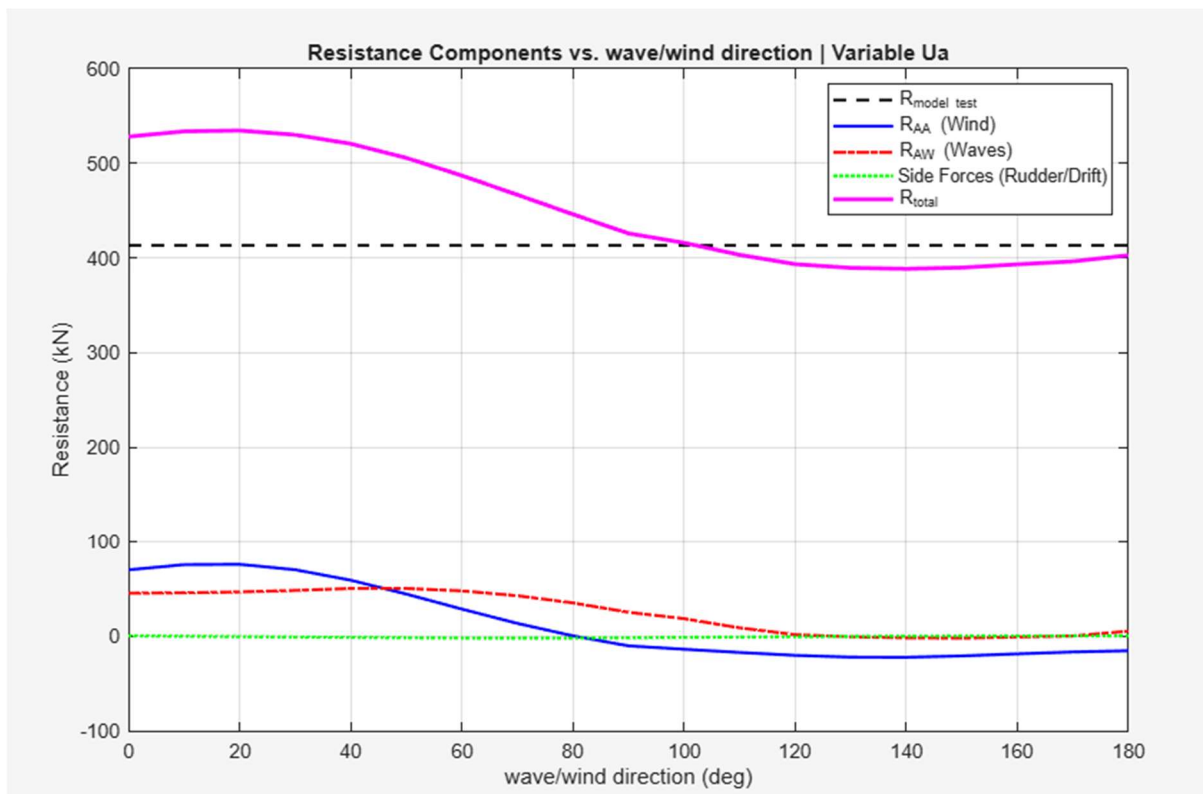


Figure 28: Total Resistance Components for Scenario 1 – Variable U_a , No eSAIL

Scenario 2

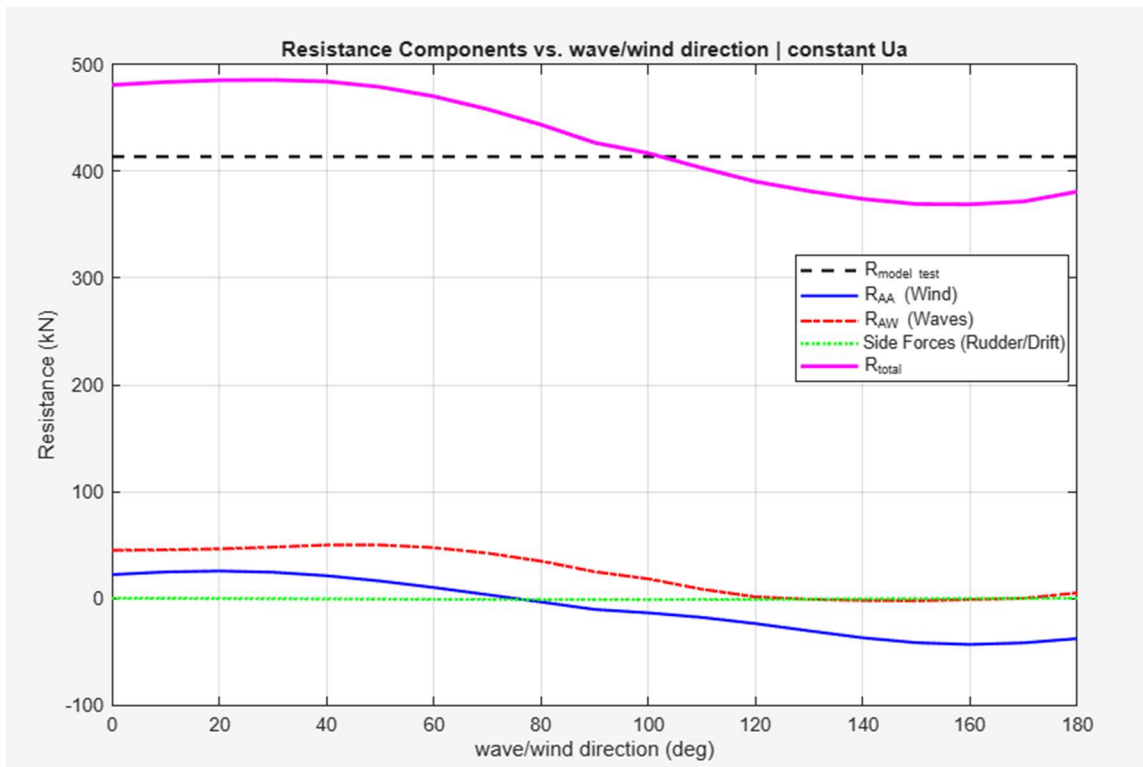


Figure 29: Total Resistance Components for Scenario 2 – Constant U_a, No eSAIL

Scenario 3

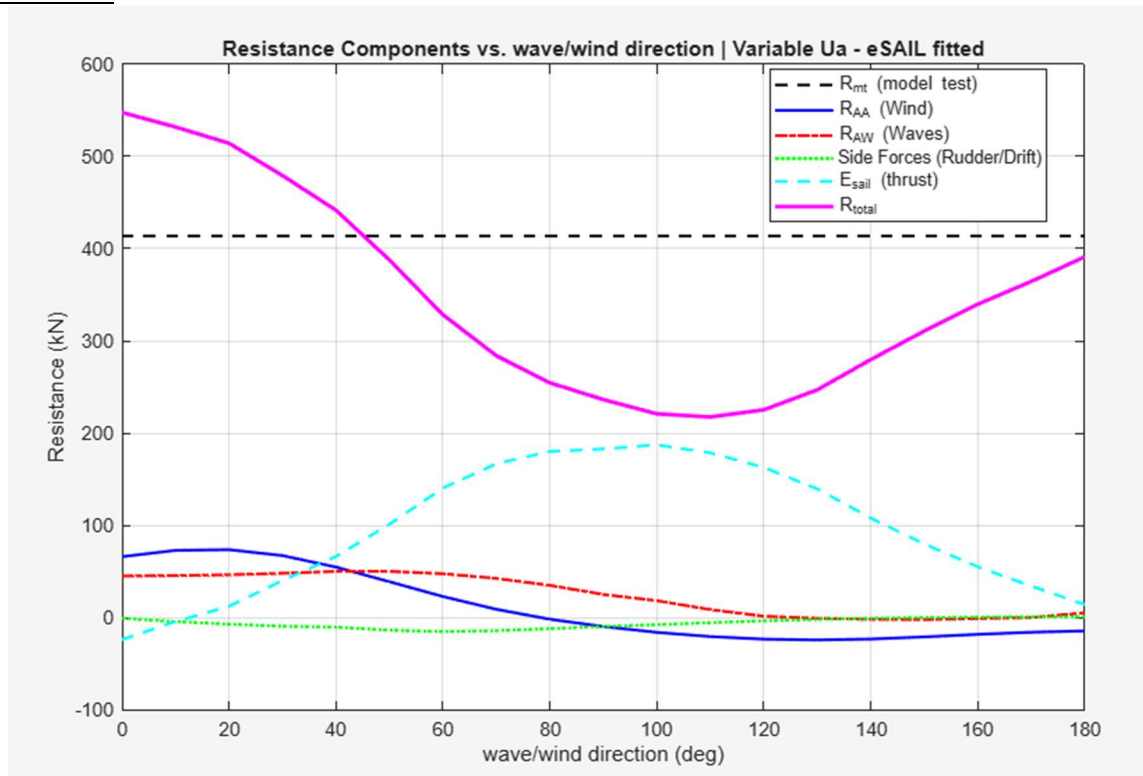


Figure 30: Total Resistance Components for Scenario 3 – Variable U_a, With eSAIL

Scenario 4

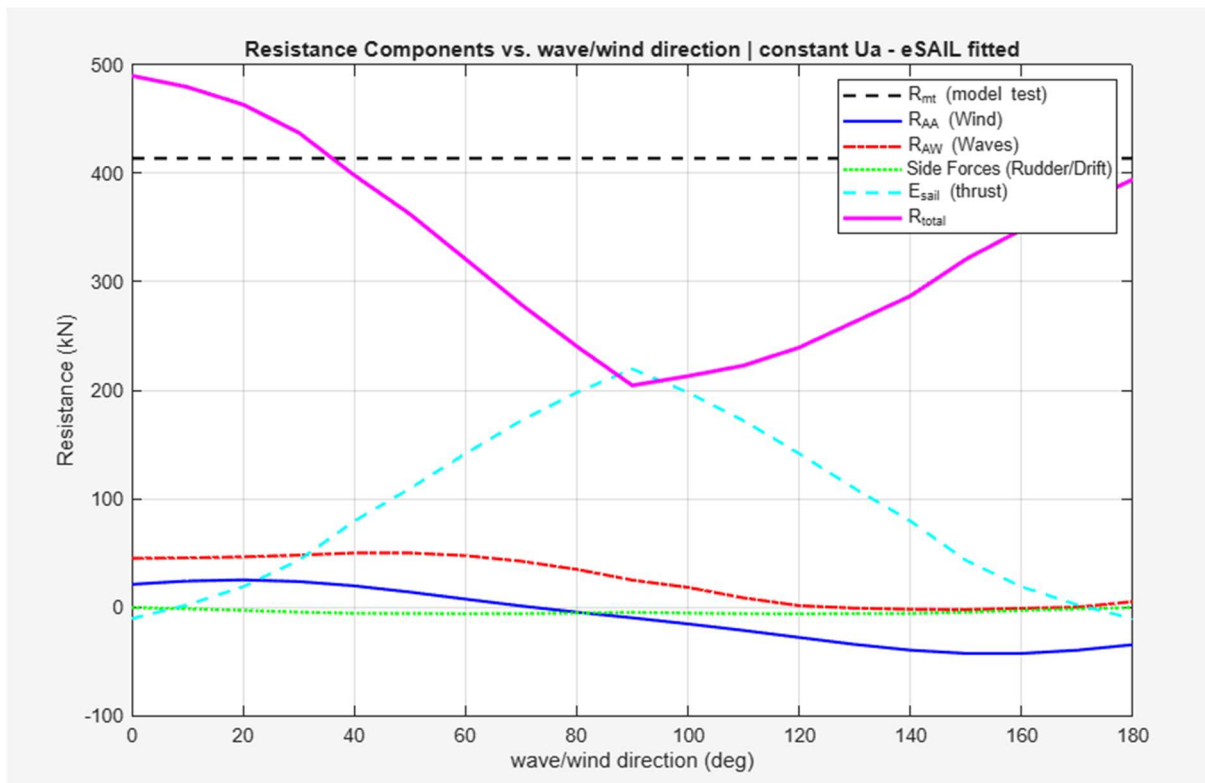


Figure 31: Total Resistance Components for Scenario 4 – Constant U_a , With eSAIL

To provide a comprehensive comparison, a combined plot of total resistance (R_{total}) was prepared. This plot illustrates the variation of resistance across all examined scenarios and heading angles, allowing for clearer assessment of the effects of eSAIL operation and apparent wind conditions.

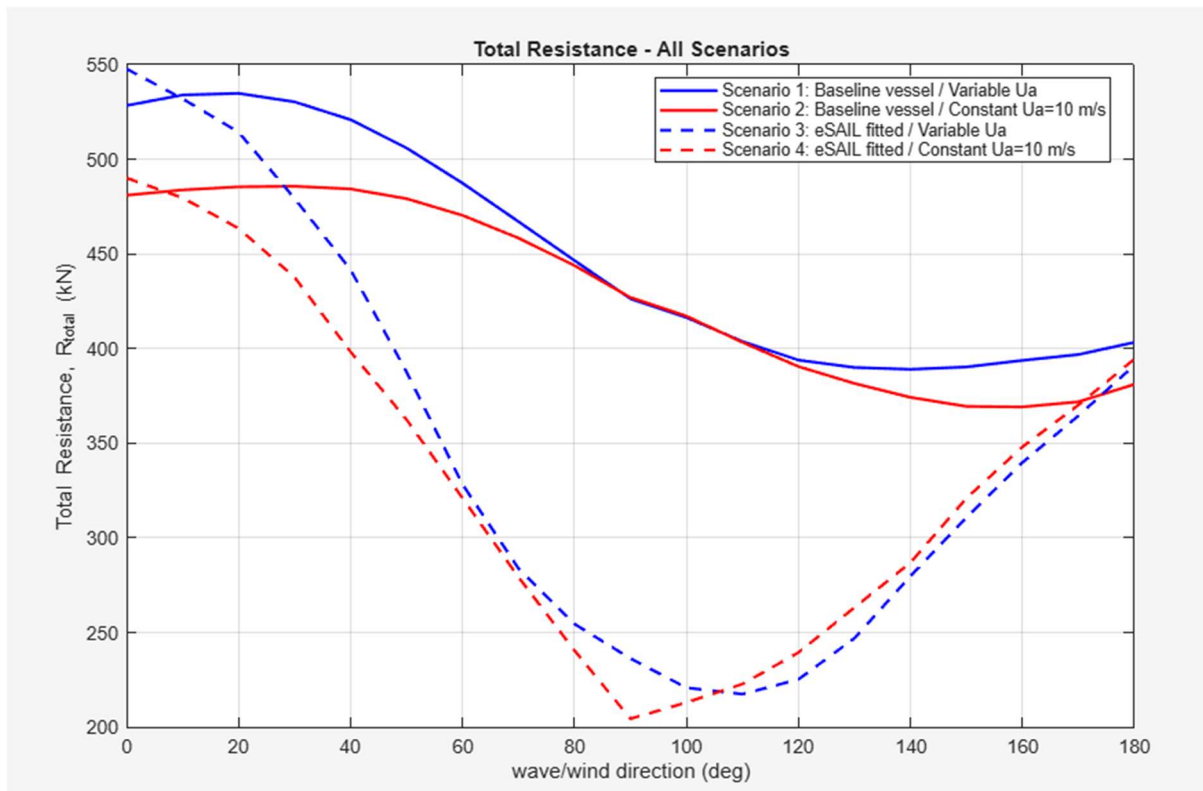


Figure 32: Total Resistance versus Wave/Wind Direction under Different Apparent Wind Conditions for Baseline and eSAIL-Fitted Vessel

4.5 Power Requirements for Defined Scenarios

Based on the total resistance results presented in previous section, the corresponding power demand is derived according to the propulsion relations described in Sections 3.3.1 and 3.3.2, which link total resistance to propeller thrust and delivered power.

The plot compares the Total Required Power across all four operational scenarios, highlighting the influence of the eSAIL system on propulsion demand. Consistent with the power integration approach described in Section 3.3.3, the total power includes both the Main Engine load and the auxiliary consumption of the eSAIL units. Results show that when the eSAILS operate, the power is notably reduced—especially at favourable wind angles—confirming the system’s contribution to lowering overall energy demand.

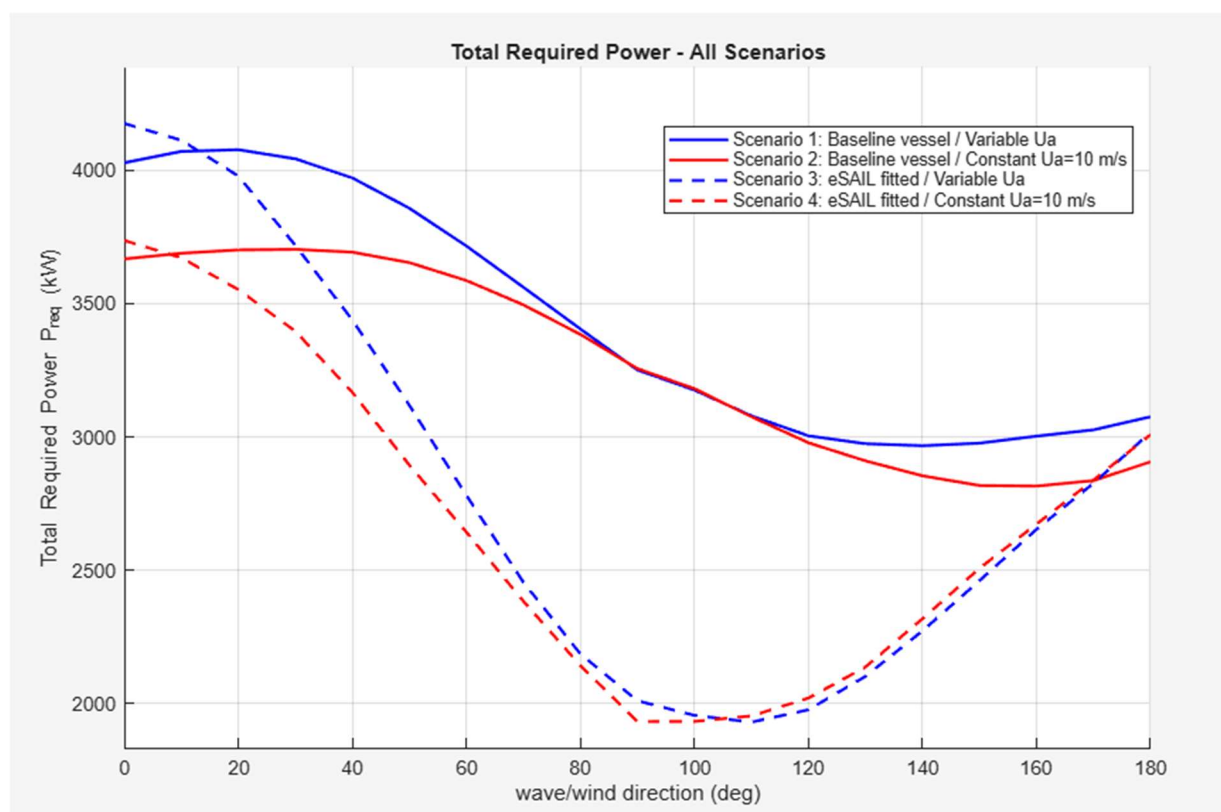


Figure 33: Total Required Power versus Wave/Wind Direction under Different Apparent Wind Conditions for Baseline and eSAIL-Fitted Vessel

4.6 Specific Fuel Oil Consumption

To support the analysis of engine performance under the different scenarios, the specific fuel oil consumption (SFOC) values obtained from the shop test of the main engine are presented in Table 4. These values serve as the reference for evaluating fuel consumption across the four defined scenarios. (Reference: MAIN Engine SHOP TEST, [50])

Table 4: Specific Fuel Oil Consumption versus Engine load

Engine Load (%)	SFOC (g/kWh)
25	175.85
35	172.75
50	167.68
71.6	165.96
75	167.65
100	172.6
110	174.94

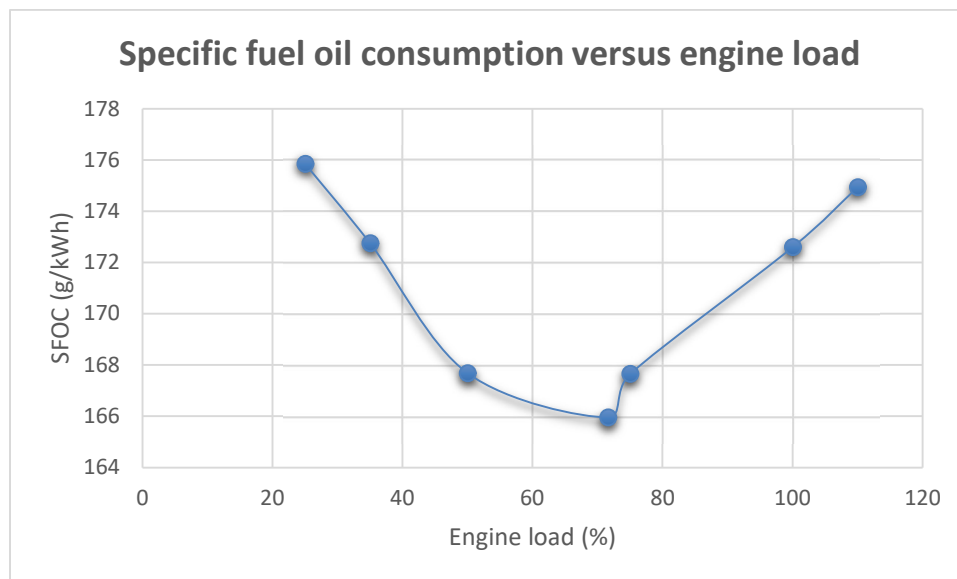


Figure 34: Specific Fuel Oil Consumption versus Engine load

For the calculation of fuel consumption resulting from the auxiliary power demand of the eSAIL units, a specific fuel oil consumption for auxiliary engines (SFOC_{AE}) of 220 g/kWh has been assumed in this thesis.

4.7 Fuel Consumption Comparison

The daily fuel consumption for each operational scenario was estimated by combining the specific fuel oil consumption (SFOC) values of Section 4.6 with the corresponding propulsion power demand obtained from the analysis. The resulting plot presents the variation of total daily fuel use with wind direction under different apparent wind conditions. The baseline cases, representing operation without eSAIL assistance, show consistently higher fuel consumption across most headings. When the eSAIL system is active, the total fuel demand decreases, resulting in noticeable fuel reductions— clearly visible at angles between 60° and 120° , where the sails are most effective. The comparison between variable and constant apparent wind cases highlights that accounting for wind variation produces smoother and more realistic fuel consumption profiles.

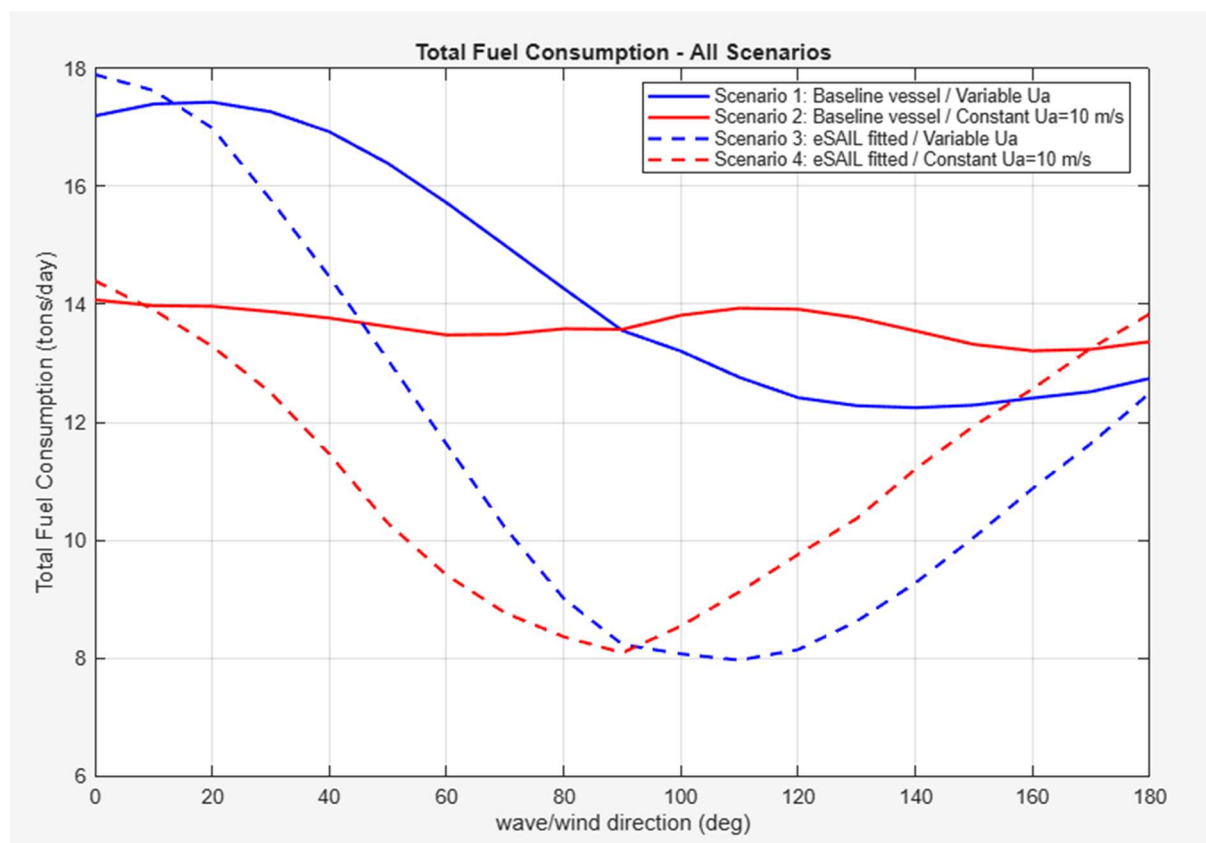


Figure 35: Total Daily Fuel Consumption versus Wave/Wind Direction under Different Apparent Wind Conditions for Baseline and eSAIL-Fitted Vessel

The corresponding fuel savings, expressed as a percentage reduction between the eSAIL-fitted and baseline configurations, are presented below. These results quantify the benefit of the wind-assisted system by comparing total daily fuel use across the four operational scenarios.

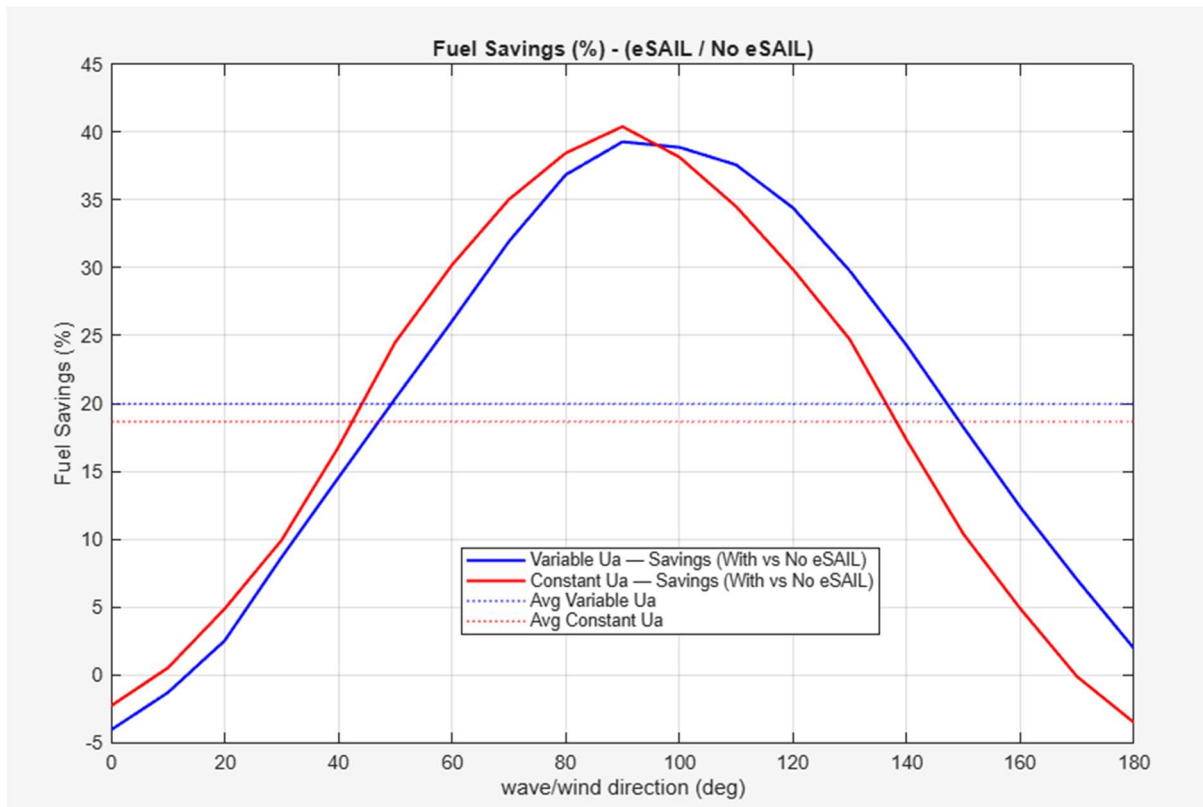


Figure 36: Fuel Savings in (%) versus Wave/Wind Direction under Different Apparent Wind Conditions for Baseline and eSAIL-Fitted Vessel

Average fuel savings across heading angles (0–180°):

- Variable Ua – 19.96%
- Constant Ua – 18.66%

Maximum fuel savings across heading angles (0–180°):

- Variable Ua – 39.3 %
- Constant Ua – 40.4 %

The two curves follow a similar trend, but their peaks occur at slightly different headings. Under variable apparent wind conditions, the maximum savings appear at intermediate angles between beam and quartering conditions (around 90°–130°), where the combined effect of true and apparent wind vectors enhances the aerodynamic contribution of the eSAILS. In contrast, the constant-wind scenario shows a more symmetrical pattern across heading angles.

4.8 Fuel Savings in Different Sea States

This section extends the analysis beyond the reference condition of a fixed true wind speed ($U_t = 10$ m/s) by incorporating different sea states derived from the Beaufort scale. The objective is to evaluate how varying wind and wave conditions influence the vessel's fuel-saving performance when equipped with the eSAIL system.

Table 5: Beaufort Scale of Wind – Representative Sea States [ITTC, 2021 Sea Trials]

BEAUFORT SCALE			
No.	Descriptive Term	Mean Wind Speed, U_t (m/s)	Probable Wave Height, H_s (m)
4	Moderate breeze	6.7	1.0
6	Strong breeze	12.3	3.0

Two representative sea states corresponding to Beaufort numbers 4 and 6 are considered, covering moderate and strong breeze conditions. For each case, the associated mean wind speed and probable wave height, as defined in the Beaufort scale, are applied to establish realistic operating environments. These conditions are used to compute and visualize the variation of fuel savings with wind incidence angle. The resulting polar plots provide a comparative illustration of how eSAIL performance evolves under increasingly energetic sea states, reflecting its capability to deliver consistent fuel reduction across a broad spectrum of environmental conditions.

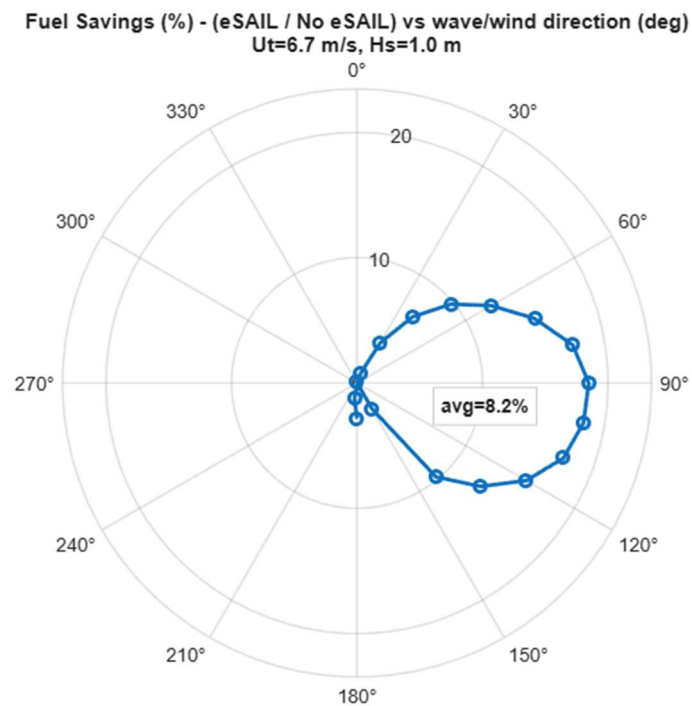
BF 4: Moderate breeze

Figure 37: Polar Plot of Fuel Savings across Wave/Wind Angles under Beaufort 4 (Moderate Breeze) Conditions for Baseline and eSAIL-Fitted Vessel

For Beaufort 4 ($U_t = 6.7$ m/s, $H_s = 1.0$ m), the eSAIL achieves an average fuel saving of $\approx 8.2\%$. The highest savings appear between 70° and 110° , showing the most effective range of operation.

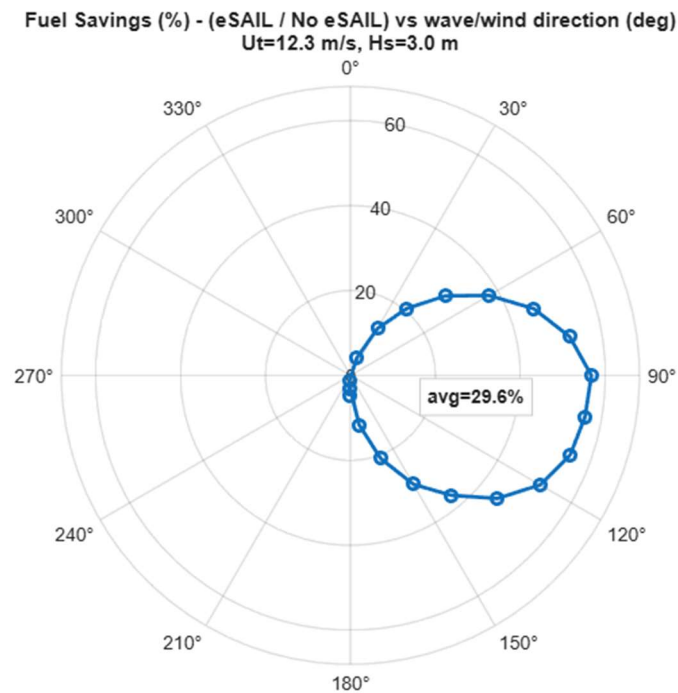
BF 6: Strong breeze

Figure 38: Polar Plot of Fuel Savings across Wave/Wind Angles under Beaufort 6 (Strong Breeze) Conditions for Baseline and eSAIL-Fitted Vessel

For Beaufort 6 ($U_t = 12.3$ m/s, $H_s = 3.0$ m), the eSAIL achieves an average fuel saving of $\approx 29.6\%$. This represents a clear increase compared to previous sea state, with higher savings maintained across a wider angle range.

To facilitate a direct comparison between sea states, the individual polar plots are consolidated in a single figure. This combined representation enables the evaluation of how fuel-saving performance evolves with increasing wave energy and apparent wind intensity, emphasizing the overall consistency of the eSAIL system across diverse operating environments.

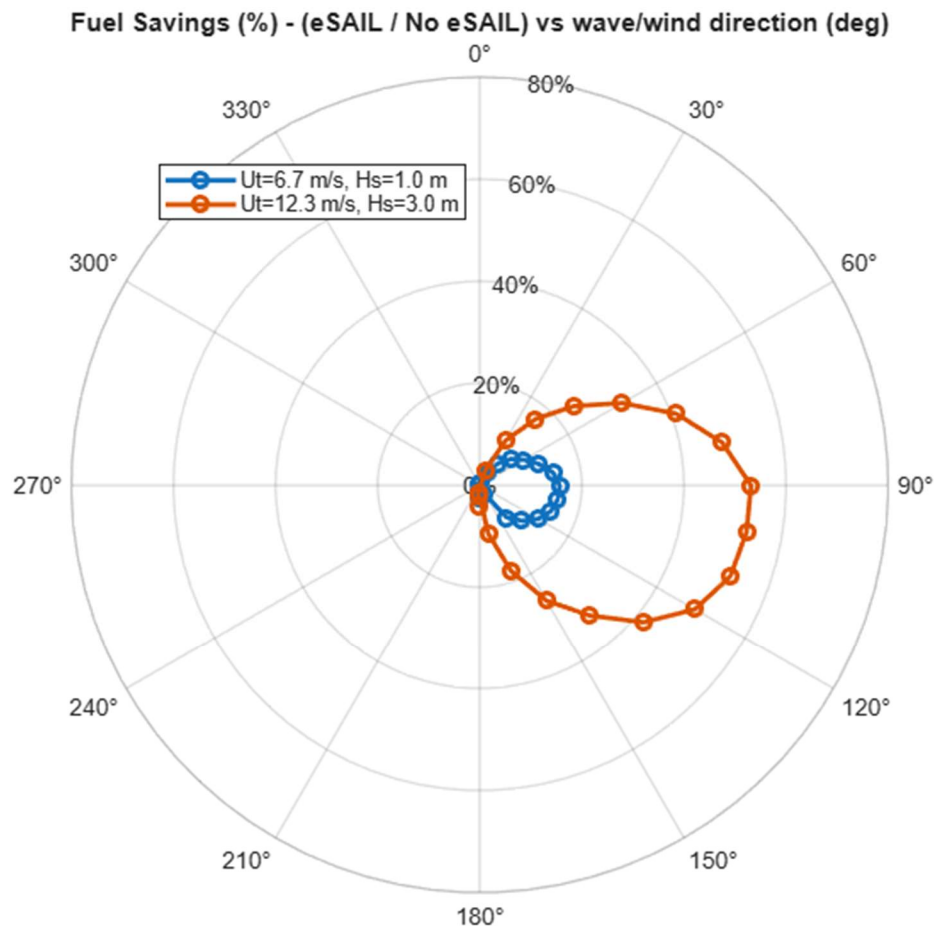


Figure 39: Combined Polar Plot of Fuel Savings across Wave/Wind Angles for Different Sea States (Beaufort 4 and 6) under Baseline and eSAIL-Fitted Conditions

The combined results show a steady increase in average fuel savings from Beaufort 4 to 6, confirming that stronger winds and higher sea states enhance the eSAIL's contribution while maintaining a consistent angle of peak performance.

Chapter 5: Conclusions and Future Research

5.1 Main Conclusions of the Thesis

This thesis investigated the potential of Wind-Assisted Propulsion Systems (WASP) as a practical approach to reduce fuel consumption and greenhouse-gas emissions in line with the objectives of the IMO's GHG reduction strategy. The study focused on the broader need for integrating renewable energy sources into conventional ship propulsion to achieve measurable efficiency improvements. Wind assistance was examined as a sustainable means of supplementing engine power, thereby decreasing dependence on fossil fuels and contributing to the transition toward cleaner maritime operations.

The analysis demonstrated that the suction-based eSAIL system effectively harnessed wind energy to generate auxiliary thrust, thereby relieving part of the load on the main engine. This reduction in propulsion demand directly translated into lower power requirements and fuel consumption, aligning with the broader objective of reducing greenhouse gas emissions in maritime transport. The system's suction-assisted airflow mechanism enhanced aerodynamic performance by increasing lift and reducing drag, which contributed to the overall improvement in propulsive efficiency observed throughout the study.

Theoretical Modeling: The theoretical framework developed in this thesis, including the baseline model without wind assistance and the modified configuration with the eSAIL system, provided a consistent basis for evaluating ship propulsion performance. The model accounted for the main resistance components —calm water resistance, added wind and wave resistance, side forces from rudder deflection & drift— and integrated the aerodynamic thrust generated by the eSAIL units. The incorporation of these factors enabled realistic estimation of total resistance, required power, and fuel consumption across different headings and operating conditions.

Influence of Resistance Sub-components: The analysis emphasised the importance of accounting for all resistance components and their combined influence on vessel performance. Calm-water resistance was the main contributor to total resistance, while added wind and wave resistances increased with heading angle. The integration of side forces, arising from drift and rudder deflection, proved essential for representing the ship's balance and course stability in crosswind conditions. These forces, though relatively small compared with the primary resistance terms, introduced additional resistance that slightly reduced the net benefit of the eSAIL thrust. Their inclusion demonstrated that wind-assisted devices modify the vessel's total resistance profile and must therefore be evaluated together with the control forces required to maintain heading. By capturing these effects within the model, the analysis provided a more realistic prediction of power demand and fuel consumption for both baseline and eSAIL-fitted conditions.

Fuel Reduction and Key Performance Results: The comparison of the four operational scenarios demonstrated a consistent reduction in propulsion power and daily fuel consumption when the eSAIL system was active. The maximum savings reached 39.3 % under variable apparent wind and 40.4 % under constant apparent wind, occurring in beam-to-quartering winds, specifically between 70° and 110°, where the aerodynamic thrust contribution was most effective. The corresponding average daily fuel savings were 20 % and 18.7 %, respectively, confirming the consistent benefit of suction-assisted propulsion across all headings.

When the analysis was extended to different sea states, the mean fuel savings across three conditions from the Beaufort scale, with progressively higher wind speed and sea severity, increased from 8.2 % to 29.6 % in the most severe case. As wind speed and wave height intensified, the relative advantage of the eSAIL system became more evident, since the generated thrust helped offset the additional resistance caused by rougher sea conditions. Overall, the study verified that suction-assisted propulsion can substantially reduce the total required power and fuel consumption and improve vessel efficiency under a wide range of operating environments.

5.2 Relation to Previous Studies

The findings of this thesis align well with the established theoretical understanding of wind-assisted propulsion and with results reported in recent studies on suction-based and rotor-type systems. The pattern of fuel savings peaking at beam and quartering winds agrees with the expected aerodynamic behaviour, where the lift-to-drag ratio of the sail-generated thrust is maximised. The use of angle-dependent aerodynamic coefficients was essential in reproducing realistic variations of forces and moments with heading angle, confirming observations from prior experimental and numerical research.

Overall, the results are consistent with recognised aerodynamic principles and previously published performance assessments of modern Wind-Assisted Propulsion Systems. The analysis across different headings and operating scenarios validated the reliability of the modelling framework and confirmed that suction-assisted sails can deliver measurable efficiency improvements under realistic operating conditions.

5.3 Future Research Directions

The methodology and results of this thesis provide a strong foundation for further work on the evaluation and optimization of wind-assisted propulsion. Future research could focus on several key areas:

Model validation and refinement: Experimental or CFD studies could be performed to validate the aerodynamic coefficients and the predicted side-force behaviour of the eSAIL. Such data would allow calibration of the current model and improved confidence in lift- and drag-force estimation.

Dynamic and voyage-scale analysis: Extending the steady-state approach to time-dependent simulations would enable assessment of eSAIL performance over complete routes using realistic wind and wave conditions, leading to annualised fuel-saving estimates.

Techno-economic assessment: Integrating the power and fuel-consumption results with cost, emission, and maintenance data would provide payback and life-cycle analyses to support investment and fleet-planning decisions.

Design and operational optimization: Future studies could investigate the influence of sail number, placement, and control strategy on overall efficiency and maneuverability, identifying optimal configurations for different vessel types.

Hybrid and regulatory integration: Combining suction sails with other Energy-Saving Devices (ESDs) and evaluating the combined effect on efficiency indices such as EEXI and CII would further support compliance with forthcoming decarbonization targets.

In conclusion, the application of suction-based wind-assisted technologies such as the eSAIL represents a practical and forward-looking step toward a more sustainable maritime sector. By harnessing wind energy to complement conventional propulsion, these systems can reduce fuel consumption and emissions while supporting the industry's long-term decarbonization goals. As innovation and regulatory momentum continue to advance, wind-assisted propulsion is expected to play an increasingly important role in shaping the next generation of energy-efficient ship designs.

References

- [1]. N. Arish, M.J. Kamper and R.J.Wang (2024). Advancements in electrical marine propulsion technologies. [Retrieved from: <https://ieeexplore.ieee.org/abstract/document/10755059/>]
- [2]. Julio Barreiro, Sonia Zaragoza, Vicente Diaz-Casas, *Science Direct*. (2022). Review of ship energy efficiency. [Retrieved from: <https://www.sciencedirect.com/science/article/pii/S002980182200960X>]
- [3]. IMO (2021). Improving the energy efficiency of ships. [Retrieved from: <https://www.imo.org/en/ourwork/environment/pages/improving%20the%20energy%20efficiency%20of%20ships.aspx>]
- [4]. Springer (2018): Barriers for adoption of energy efficiency operational measures in shipping industry. [Retrieved from: <https://link.springer.com/article/10.1007/s13437-018-0138-3>]
- [5]. Jimenez, Kim, Munim (2022): A review of ship energy efficiency research and directions towards emission reduction in the maritime industry. [Retrieved from: [A review of ship energy efficiency research and directions towards emission reduction in the maritime industry - ScienceDirect](#)]
- [6]. Tang, Moldanová (2020): The impact of ship emissions on air quality and human health in the Gothenburg area – Part 1: 2012 emissions. [Retrieved from: [ACP - The impact of ship emissions on air quality and human health in the Gothenburg area – Part 1: 2012 emissions](#)]
- [7]. Johnson, H., Andersson, K. Barriers to energy efficiency in shipping. *WMU J Marit Affairs* 15, 79–96 (2016). [Retrieved from: [Barriers to energy efficiency in shipping | WMU Journal of Maritime Affairs](#)]
- [8]. Öztürk, E. (2013). Operational Measures For Energy Efficiency In Shipping. *JEMS Maritime Sci*, 1(2), 65-72. [Retrieved from: [Operational Measures For Energy Efficiency In Shipping \[JEMS Maritime Sci\]](#)]
- [9]. Fabian Tilling, Wengang Mao, Jonas W., Ringsberg (2015): Systems modelling for energy-efficient shipping. Calmers University of Technology, Department of Shipping and Marine Technology. [Retrieved from: <https://core.ac.uk/download/pdf/70610062.pdf>]
- [10]. IMO (2025): IMO approves net-zero regulations for global shipping. [Retrieved from: <https://www.imo.org/en/mediacentre/pressbriefings/pages/imo-approves-netzero-regulations.aspx>]
- [11]. Christina Aleixendri (2025): bound4blue secures DNV validation for wind propulsion performance methodology, unlocking regulatory and commercial benefits. [Retrieved from: [bound4blue secures DNV validation for wind propulsion performance methodology, unlocking regulatory and commercial benefits | bound4blue](#)]
- [12]. Thalassinos (2025). Evaluating the impact of wind-assisted propulsion systems on ship energy efficiency. [Retrieved from <https://dspace.lib.ntua.gr/xmlui/bitstream/handle/123456789/61130/DIPLOMA%20THESIS.pdf?sequence=6>]
- [13]. Odfjell Advances Wind Propulsion with First eSAIL Installation. [Retrieved from: <https://www.environmentenergyleader.com/stories/odfjell-installs-esail-wind-propulsion-on-bow-olympus,68061>]
- [14]. Thomann (2025). Bound4blue: The return of sails in modern shipping. [Retrieved from: <https://www.juliusbaer.com/en/insights/future-insights/energy-transition/bound4blue-the-return-of-sails-in-modern-shipping/>]

- [15]. Banawan AA, El Gohary MM, Sadek IS. Environmental and economical benefits of changing from marine diesel oil to natural-gas fuel for short-voyage high-power passenger ships. *Proceedings of the Institution of Mechanical Engineers, Part M: Journal of Engineering for the Maritime Environment*. 2009;224(2):103-113. [Retrieved from: <https://journals.sagepub.com/doi/abs/10.1243/14750902JEME181>]
- [16]. UNCTAD (2023). Review of Maritime Transport 2023 – Towards Decarbonized Shipping. [Retrieved from: <https://unctad.org/publication/review-maritime-transport-2023>]
- [17]. Naida Hakirevic Prevljak (2024). Wind ship propulsion in maritime: 2024 was a year to remember. [Retrieved from: [Wind ship propulsion in maritime: 2024 was a year to remember - Offshore Energy](#)]
- [18]. Y Remyha *et al* 2023 *IOP Conf. Ser.: Earth Environ* (2023). Energy-saving technologies for sustainable development of the maritime transport logistics market. [Retrieved from: [Energy-saving technologies for sustainable development of the maritime transport logistics market - IOPscience](#)]
- [19]. IEA (2025), How the shipping sector could save on energy costs, IEA, Paris [Retrieved from: <https://www.iea.org/commentaries/how-the-shipping-sector-could-save-on-energy-costs>]
- [20]. Erica Sembrano (2025). The Future of Marine Propulsion: Why Go Electric? [Retrieved from: [The Future of Marine Propulsion: Why Go Electric? – Momentum Electric Marine](#)]
- [21]. Crist, Philippe (2009). Greenhouse gas emissions reduction potential from international shipping. [Retrieved from: [EconStor: Greenhouse gas emissions reduction potential from international shipping](#)]
- [22]. Environ. Sci. Technol. (2009). Shipping Emissions: From Cooling to Warming of Climate – and Reducing Impacts on Health. [Retrieved from: [Shipping Emissions: From Cooling to Warming of Climate—and Reducing Impacts on Health | Environmental Science & Technology](#)]
- [23] International Towing Tank Conference (ITTC). (2021). *Preparation, Conduct and Analysis of Speed/Power Trials (7.5-04-01-01.1, Rev. 06)*. ITTC – Recommended Procedures and Guidelines. [Retrieved from: <https://www.itc.info/media/9874/75-04-01-011.pdf>]
- [24]. ESCAP: Decarbonizing shipping and maritime connectivity. [Retrieved from: <https://unescap.org/projects/regional-initiative-ocean-based-climate-action/decarbonizing-shipping-maritime-connectivity>]
- [25]. Melnyk O., Onishchenko, O., & Onyschenko, S. (2023). Renewable energy concept development and application in shipping industry. [Retrieved from: [Renewable Energy Concept Development and Application in Shipping Industry 9 Lex Portus 2023](#)]
- [26]. International Maritime Organization (2020): Fourth IMO GHG Study. [Retrieved from: https://greenvoyage2050.imo.org/wp-content/uploads/2021/07/Fourth-IMO-GHG-Study-2020-Full-report-and-annexes_compressed.pdf.]
- [27]. International Maritime Organization (2018): Adoption of the Initial IMO Strategy on Reduction of GHG Emissions from Ships [Retrieved from: [https://wwwcdn.imo.org/localresources/en/KnowledgeCentre/IndexofIMOResolutions/MEPCDocuments/MEPC.304\(72\).pdf](https://wwwcdn.imo.org/localresources/en/KnowledgeCentre/IndexofIMOResolutions/MEPCDocuments/MEPC.304(72).pdf).]
- [28]. Rehmatulla, N., Calleya, J. & Smith, T. (2017): The implementation of technical energy efficiency and CO₂ emission reduction measures in shipping. [Retrieved from: <https://discovery.ucl.ac.uk/id/eprint/1555671>]

- [29]. Interreg North Sea Region (2023): WASP – Wind Assisted Ship Propulsion Project. Σύνδεσμος: <https://northsearegion.eu/wasp/>.
- [30]. Traut, M. et al. (2014): Propulsive power contribution of a Flettner rotor on a 190 m cargo ship. [Retrieved from: <https://ideas.repec.org/a/eee/appene/v113y2014icp362-372.html>].
- [31]. Lu, R. & Ringsberg, J.W. (2020): Ship energy performance study of three wind-assisted ship propulsion technologies using a voyage optimization tool. [Retrieved from: <https://doi.org/10.1080/17445302.2019.1612544>.]
- [32]. bound4blue (2023): Aerodynamic optimization of the eSAIL®. [Retrieved from: bound4blue.com, <https://bound4blue.com/aerodynamic-optimization-of-the-esail/>]
- [33]. Cousteau, J.-Y. & Charrier, B. (1985): The Turbosail: New propulsion for ships. Marine Technology. [Retrieved from: <https://www.cousteau.org>, <https://www.cousteau.org/know/inventions/turbosail/>]
- [34]. DNV (2024): bound4blue eSAIL® receives DNV Type Approval validating quality and accelerating adoption [Retrieved from: <https://bound4blue.com/dnv-validates-esails-qualify-safety/>]
- [35]. Tillig, F. (2021) 'Performance prediction and design of wind-assisted propulsion systems', ResearchGate. Available at: [Retrieved from: https://www.researchgate.net/publication/357166494_Performance_prediction_and_design_of_wind-assisted_propulsion_systems]
- [36]. Ortega, J. et al. (2025): eSAILs®: Using wind to improve real vessel CII and environmental performance. [Retrieved from: <https://doi.org/10.5281/zenodo.14789998>]
- [37]. Tillig, F., Ringsberg, J.W. & Mao, W. (2020): Design, operation and analysis of wind-assisted cargo ships. [Retrieved from: [Design, operation and analysis of wind-assisted cargo ships](#)]
- [38]. New Wind Propulsion Technology A Literature Review of Recent Adoptions (2020). [Retrieved from: https://vb.northsearegion.eu/public/files/repository/20210111083115_WASP-WP4.D5B-NewWPTALiteratureReviewofRecentAdoptions-Final.pdf]
- [39]. Skogman (1985) – Study in naval hydrodynamics and ship maneuvering models. [Retrieved from: https://www.academia.edu/75280826/Mathematical_model_of_the_ship_manoeuvring]
- [40]. Elger (2019) – Contemporary study applying methodologies from Fujiwara and Skogman for ship maneuvering and drift angle prediction. [Retrieved from: <https://www.sciencedirect.com/science/article/abs/pii/S0029801820310878>]
- [41]. Fujiwara (2001) – Reference to Fujiwara coefficients for ship resistance and propulsion. [Retrieved from: <https://www.itc.info/media/11900/75-02-07-028.pdf>]
- [42]. Marinoni (2024) Reviewing the Role and Effectiveness of Wind-Assisted Ship Propulsion Technology in the Maritime Industry’s Decarbonization efforts. Pdf
- [43]. Bound4blue: eSAIL [Retrieved from: <https://bound4blue.com/esail/>]
- [44]. Hopes, Pearson, Buckingham.(2021).A CFD study on wind assisted propulsion technology for commercial shipping [Retrieved from: https://www.researchgate.net/publication/355675684_A_CFD_Study_on_Wind_Assisted_Propulsion_Technology_for_Commercial_Shipping]
- [45]. Practical Estimation of Ship Propulsive Power Retrieved from: https://api.pageplace.de/preview/DT0400.9781139089203_A23866158/preview-9781139089203_A23866158.pdf

- [46]. The Principles of Naval Architecture - SNAME, Volume II (Resistance, Propulsion and Vibration)
Retrieved from: <https://navalifpe.files.wordpress.com/2011/09/principles-of-naval-architecture-vol-2-sname.pdf>
- [47]. Chapter 7 - Resistance and Powering of Ships - U.S. Naval Academy [Retrieved from: <https://www.usna.edu/NAOE/files/documents/Courses/EN400/02.07%20Chapter%207.pdf>]
- [48]. Liu, Papanikolaou, Zaraphonitis (2015). Practical approach to the added resistance of a ship in short waves. [Retrieved from: https://www.researchgate.net/publication/273342290_Practical_approach_to_the_added_resistance_of_a_ship_in_short_waves]
- [49]. TOWING TANK MODEL TEST REPORT FOR A 82000DWT BULK CARRIER WITH PSV and HVAF Retrieved from: https://ittc.info/media/5732/towing_tank.pdf
- [50]. MAIN Engine SHOP TEST [Retrieved from: https://www.classnk.com/hp/pdf/rules/amendments/eAmendments/Outline/230630/23-2-33e_outline.pdf]
- [51]. (IMO 2021a, IMO 2011, MEPC.335(76) 2021 [Retrieved from: [https://wwwcdn.imo.org/localresources/en/KnowledgeCentre/IndexofIMOResolutions/MEPCDocuments/MEPC.335\(76\).pdf](https://wwwcdn.imo.org/localresources/en/KnowledgeCentre/IndexofIMOResolutions/MEPCDocuments/MEPC.335(76).pdf)]
- [52]. WASP Project Final Report 2022 [Retrieved from: <https://northsearegion.eu/wasp/index.html>]
- [53]. Container ship with Flettner rotor ship returns to service. Ships Monthly. [Retrieved from <https://shipsmonthly.com/news/container-ships-flettner-rotor-ship-returns-to-service/>]
- [54]. Datamar News, (n.d.). Bulk carrier with rigid sails berths in Brazil for the 1st time. [Retrieved from: <https://datamarnews.com/noticias/bulk-carrier-with-rigid-sails-berths-in-brazil-for-the-1st-time>]
- [55]. Sanderson, K. (2008) 'Ship kites in to port', Nature. [Retrieved from: <https://doi.org/10.1038/news.2008.564.>]
- [56]. Odfjell first to install suction sails on deep-sea chemical tanker. Ships Monthly. [Retrieved from: <https://shipsmonthly.com/news/odfjell-first-to-install-suction-sails-on-deep-sea-chemical-tanker>]
- [57]. Kolodziejcki, M. and Sosnowski, M. (2025) 'Review of Wind-Assisted Propulsion Systems in Maritime Transport', Energies, 18(4), article number: 897. doi: 10.3390/en18040897. [Retrieved from: <https://www.mdpi.com/1996-1073/18/4/897>]
- [58.] Mallouppas, G., et al. (2024) 'Impact of Wind-Assisted Propulsion on Fuel Savings and Propeller Efficiency: A Case Study', Journal of Marine Science and Engineering, 12(11), p. 2100. doi: 10.3390/jmse12112100. [Retrieved from: <https://www.mdpi.com/2077-1312/12/11/2100.>]
- [59] J. Doe, A. Smith, and B. Johnson, "Modeling and Evaluation of Ship Propulsion with Wind-Assisted Technologies," J. Ship Res., vol. 67, no. 3, pp. 150–165, Sep. 2023, doi: 10.5957/JSR.67.3.150. [Online]. [Retrieved from: <https://www.ship-research.com/en/supplement/1c3f88ad-c451-474e-8704-415cb348bcb9>]
- [60] Shigunov, V. (2018) 'Numerical prediction of added power in seaway', Journal of Offshore Mechanics and Arctic Engineering, 140(5), p. 051102. [Retrieved from: <https://doi.org/10.1115/1.4039955>].

Appendix A: Ship Data from Towing Tank Test Report

Table 6: Propeller open-water characteristics in Scantling Draft

Propeller's open-water performance			
Particular	Symbol	Unit	Value
Diameter	D	m	6.95
J	k_T	$10 \cdot k_Q$	η_0
0	0.4045	0.4691	0
0.05	0.3941	0.4577	0.0685
0.1	0.3791	0.4417	0.1366
0.15	0.3614	0.4234	0.2037
0.2	0.342	0.4043	0.2692
0.25	0.3216	0.3849	0.3324
0.3	0.3005	0.3651	0.3929
0.35	0.2789	0.3448	0.4505
0.4	0.2568	0.3236	0.5051
0.45	0.2342	0.3014	0.5564
0.5	0.2112	0.2781	0.6042
0.55	0.1878	0.2538	0.6476
0.6	0.1639	0.2285	0.6848
0.65	0.1395	0.2024	0.7128
0.7	0.1145	0.1754	0.727
0.75	0.0884	0.1467	0.719

Table 7: Self Propulsion factors for Scantling Draft

Scantling Draft (14.45m)					
V (kn)	t	w	η_r	C_P	C_N
10	0.193	0.261	1.035	0.99	1
10.5	0.193	0.261	1.035		
11	0.193	0.261	1.035		
11.5	0.193	0.261	1.035		
12	0.182	0.255	1.015		
12.5	0.178	0.253	1.012		
13	0.178	0.253	1.015		
13.5	0.179	0.253	1.015		
14	0.176	0.251	1.014		
14.5	0.168	0.248	1.014		
15	0.179	0.254	1.014		
15.5	0.179	0.254	1.014		

Appendix B: Added resistances

B.1 Added wave and wind resistances

B.1.1 Added wind resistance - Fujiwara regression formula

For the wind resistance coefficient C_{DA} , the Fujiwara regression formula [23, p.51] can be used. According to this formula:

$$C_{DA} = C_{LF} \cdot \cos \psi_a + C_{XLI} \cdot \left(\sin \psi_a - \frac{1}{2} \cdot \sin \psi_a \cdot \cos^2 \psi_a \right) \cdot \sin \psi_a \cdot \cos \psi_a + C_{ALF} \cdot \sin \psi_a \cdot \cos^3 \psi_a$$

With:

for $0 \leq \psi_a < 90$ (deg.)

$$C_{LF} = \beta_{10} + \beta_{11} \cdot \frac{A_{YV}}{L_{OA} \cdot B} + \beta_{12} \cdot \frac{C_{MC}}{L_{OA}}$$

$$C_{XLI} = \delta_{10} + \delta_{11} \cdot \frac{A_{YV}}{L_{OA} \cdot h_{BR}} + \delta_{12} \cdot \frac{A_{XV}}{B \cdot h_{BR}}$$

$$C_{ALF} = \varepsilon_{10} + \varepsilon_{11} \cdot \frac{A_{OD}}{A_{YV}} + \varepsilon_{12} \cdot \frac{B}{L_{OA}}$$

for $90 \leq \psi_a < 180$ (deg.)

$$C_{XLI} = \delta_{20} + \delta_{21} \cdot \frac{A_{YV}}{L_{OA} \cdot h_{BR}} + \delta_{22} \cdot \frac{A_{XV}}{A_{YV}} + \delta_{23} \cdot \frac{B}{L_{OA}} + \delta_{24} \cdot \frac{A_{XV}}{B \cdot h_{BR}}$$

$$C_{LF} = \beta_{20} + \beta_{21} \cdot \frac{B}{L_{OA}} + \beta_{22} \cdot \frac{h_C}{L_{OA}} + \beta_{23} \cdot \frac{A_{OD}}{L_{OA}^2} + \beta_{24} \cdot \frac{A_{XV}}{B^2}$$

$$C_{ALF} = \varepsilon_{20} + \varepsilon_{21} \cdot \frac{A_{OD}}{A_{YV}}$$

for $\psi_a = 90$ (deg.)

$$C_{DA}|_{\psi_a=90(\text{deg.})} = \frac{1}{2} \cdot (C_{DA}|_{\psi_a=90(\text{deg.})-\mu} + C_{DA}|_{\psi_a=90(\text{deg.})+\mu})$$

Where:

A_{OD} : lateral projected area of superstructures etc. on deck,

A_{XV} : area of maximum transverse section exposed to the winds,

A_{YV} : projected lateral area above the waterline,

B : ship breadth,

C_{DA} : wind resistance coefficient,

C_{MC} : horizontal distance from midship section to centre of lateral projected area A_{YV} ,

h_{BR} : height of top of superstructure (bridge etc.),

h_C : height from waterline to centre of lateral projected area A_{YV} ,

L_{OA} : length overall,

μ : smoothing range; normally 10 (deg.),

ψ_a : smoothing range; normally 10 (deg.),

Non-dimensional parameters β_{ij} , δ_{ij} and ε_{ij} are defined below.

Table 8: Non-dimensional parameters [23, Tbl. F-2]

	i	j				
		0	1	2	3	4
β_{ij}	1	0.922	-0.507	-1.162	-	-
	2	-0.018	5.091	-10.367	3.011	0.341
δ_{ij}	1	-0.458	-3.245	2.313	-	-
	2	1.901	-12.727	-24.407	40.31	5.481
ε_{ij}	1	0.585	0.906	-3.239	-	-
	2	0.314	1.117	-	-	-

The parameters that need to be inputted in regression formula by Fujiwara are portrayed in the following figure.

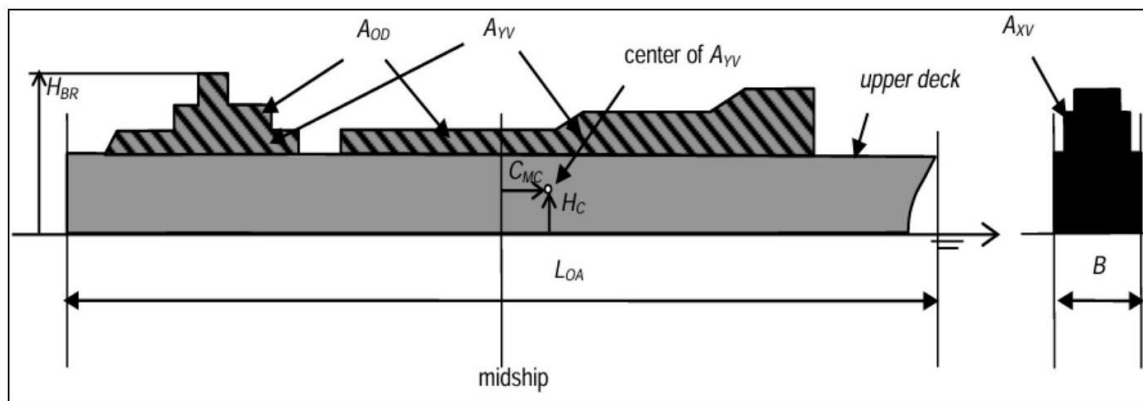


Figure 40: Input parameters for regression formula by Fujiwara

B.1.2 Methodology for Calculation of Fujiwara Coefficients (C_Y , C_N)

$$C_X = X_0 + X_1 \cos \psi + X_3 \cos 3\psi + X_5 \cos 5\psi \quad (3.28)$$

$$C_Y = Y_1 \sin \psi + Y_3 \sin 3\psi + Y_5 \sin 5\psi \quad (3.29)$$

$$C_N = N_1 \sin \psi + N_2 \sin 2\psi + N_3 \sin 3\psi \quad (3.30)$$

$$C_K = K_1 \sin \psi + K_2 \sin 2\psi + K_3 \sin 3\psi + K_5 \sin 5\psi \quad (3.31)$$

Where:

C_X = surge force coefficient,

C_Y = sway (lateral) force coefficient,

C_N = yaw moment coefficient,

C_K = roll moment coefficient,

ψ = wind incidence angle.

Each term on C_Y is expressed as follows.

$$\begin{aligned}
Y_1 &= y_{10} + y_{11} \frac{C_{BR}}{L} + y_{12} \frac{C}{L} + y_{13} \left(\frac{A_{OD}}{A_L} \right)^{-1} \\
&\quad + y_{14} \frac{C}{H_C} + y_{15} \left(\frac{BH_{BR}}{A_T} \right)^{-1} \\
Y_3 &= y_{30} + y_{31} \frac{A_L}{LB} + y_{32} \frac{LF_F}{A_L} + y_{33} \frac{C_{BR}}{L} \\
&\quad + y_{34} \left(\frac{H_{BR}}{B} \right)^{-1} + y_{35} \frac{A_{OD}}{A_L} + y_{36} \left(\frac{BH_{BR}}{A_T} \right)^{-1} \\
Y_5 &= y_{50} + y_{51} \frac{A_L}{LB} + y_{52} \left(\frac{H_{BR}}{L} \right)^{-1} + y_{53} \frac{C_{BR}}{L} \\
&\quad + y_{54} \left(\frac{A_T}{B^2} \right)^{-1} + y_{55} \frac{C}{L} + y_{56} \frac{LH_C}{A_L}
\end{aligned}$$

Each term on C_N is expressed as follows;

$$\begin{aligned}
N_1 &= n_{10} + n_{11} \frac{C}{L} + n_{12} \frac{LH_C}{A_L} + n_{13} \left(\frac{A_L}{A_T} \right)^{-1} + n_{14} \frac{C}{H_C} \\
&\quad + n_{15} \frac{A_L}{LB} + n_{16} \frac{A_T}{L^2} + n_{17} \left(\frac{A_T}{B^2} \right)^{-1} + n_{18} \frac{C_{BR}}{L} \\
N_2 &= n_{20} + n_{21} \frac{C_{BR}}{L} + n_{22} \frac{C}{L} + n_{23} \left(\frac{A_{OD}}{A_L} \right)^{-1} \\
&\quad + n_{24} \frac{A_T}{B^2} + n_{25} \left(\frac{H_{BR}}{L} \right)^{-1} + n_{26} \left(\frac{BH_{BR}}{A_T} \right)^{-1} \\
&\quad + n_{27} \frac{A_L}{LB} + n_{28} \frac{A_L}{L^2} \\
N_3 &= n_{30} + n_{31} \frac{C_{BR}}{L} + n_{32} \left(\frac{BH_{BR}}{A_T} \right)^{-1} + n_{33} \frac{A_L}{A_T}
\end{aligned}$$

The regression constants Y_i , N_i , are determined based on the principal particulars of the ship, including block coefficient, length-to-beam ratio, draft, and lateral projected area. For the case study vessel, these constants were extracted from the parameter tables provided in Fujiwara.

Table 9: Each coefficient of independent variables

m=		0	1	2	3	4	5	6	7	8
C_X	x_{0m}	-0.330	0.293	0.0193	0.682					
	x_{1m}	-1.353	1.700	2.87	-0.463	-0.570	-6.640	-0.0123	0.0202	
	x_{3m}	0.830	-0.413	-0.0827	-0.563	0.804	-5.67	0.0401	-0.132	
	x_{5m}	0.0372	-0.0075	-0.103	0.0921					
C_Y	y_{1m}	0.684	0.717	-3.22	0.0281	0.0661	0.298			
	y_{3m}	-0.400	0.282	0.307	0.0519	0.0526	-0.0814	0.0582		
	y_{5m}	0.122	-0.166	-0.0054	-0.0481	-0.0136	0.0864	-0.0297		
C_N	n_{1m}	0.299	1.71	0.183	-1.09	-0.0442	-0.289	4.24	-0.0646	0.0306
	n_{2m}	0.117	0.123	-0.323	0.0041	-0.166	-0.0109	0.174	0.214	-1.06
	n_{3m}	0.0230	0.0385	-0.0339	0.0023					
C_K	k_{1m}	3.63	-30.7	16.8	3.270	-3.03	0.552	-3.03	1.82	-0.224
	k_{2m}	-0.480	0.166	0.318	0.132	-0.148	0.408	-0.0394	0.0041	
	k_{3m}	0.164	-0.170	0.0803	4.92	-1.780	0.0404	-0.739		
	k_{5m}	0.449	-0.148	-0.0049	-0.396	-0.0109	-0.0726			

B.1.3 Added wave resistance

B.1.3.1 Wave reflection added resistance R_{AWR}

This part of the added wave resistance is computed using the sum:

$$R_{AWR} = \sum_{i=1}^4 R_{AWR_i}$$

With :

$$R_{AWR_1} = \frac{2.25}{4} \cdot \rho \cdot g \cdot B \cdot \zeta_\alpha^2 \cdot a_T \cdot \left\{ \sin^2 (E_1 - a) + \frac{2 \cdot \omega_0 \cdot U}{g} \cdot [\cos E_1 \cdot \cos (E_1 - a) - \cos a] \right\} \cdot \left(\frac{0.87}{C_B} \right)^{1+4 \cdot \sqrt{Fr}}$$

$$R_{AWR_2} = \frac{2.25}{4} \cdot \rho \cdot g \cdot B \cdot \zeta_\alpha^2 \cdot a_T \cdot \left\{ \sin^2 (E_1 + a) + \frac{2 \cdot \omega_0 \cdot U}{g} \cdot [\cos E_1 \cdot \cos (E_1 + a) - \cos a] \right\} \cdot \left(\frac{0.87}{C_B} \right)^{1+4 \cdot \sqrt{Fr}}$$

$$R_{AWR_3} = -\frac{2.25}{4} \cdot \rho \cdot g \cdot B \cdot \zeta_\alpha^2 \cdot a_T \cdot \left\{ \sin^2 (E_2 + a) + \frac{2 \cdot \omega_0 \cdot U}{g} \cdot [\cos E_2 \cdot \cos (E_2 + a) - \cos a] \right\} \cdot \left(\frac{0.87}{C_B} \right)^{1+4 \cdot \sqrt{Fr}}$$

$$R_{AWR_4} = -\frac{2.25}{4} \cdot \rho \cdot g \cdot B \cdot \zeta_\alpha^2 \cdot a_T \cdot \left\{ \sin^2 (E_2 - a) + \frac{2 \cdot \omega_0 \cdot U}{g} \cdot [\cos E_2 \cdot \cos (E_2 - a) - \cos a] \right\} \cdot \left(\frac{0.87}{C_B} \right)^{1+4 \cdot \sqrt{Fr}}$$

Where:

ρ : seawater density in $[\text{kg}/\text{m}^3]$

g : acceleration due to gravity in $[\text{m}/\text{s}^2]$

B : ship breadth in $[\text{m}]$

ζ_α : wave amplitude $[\text{m}]$

$$a_T = \begin{cases} 1 - e^{-4 \cdot \pi \cdot \left(\frac{T^* - T^*}{\lambda - 2.5 \cdot L_{pp}}\right)}, & \frac{\lambda}{L_{pp}} \leq 2.5 \\ 0, & \frac{\lambda}{L_{pp}} > 2.5 \end{cases}$$

λ : wave length in $[\text{m}]$

For cases 1 and 2,

$$T^* = T_{\max} \text{ but for cases 3 and 4, } T^* = \begin{cases} \frac{T_{\max} \cdot (4 + \sqrt{|\cos a|})}{5}, & \text{for } C_B \leq 0.75 \\ \frac{T_{\max} \cdot (2 + \sqrt{|\cos a|})}{5}, & \text{for } C_B > 0.75 \end{cases}$$

ω_0 : angular velocity of wave in $[\text{rad}/\text{s}]$

U : ship speed in $[\text{m}/\text{s}]$

a : is the angle of the wave, in $[\text{rad}]$, with 0 being the bow waves and π being the following waves

Fr: is the Froude number of the ship

E_1, E_2 : are the angles, in $[\text{rad}]$, shown in the picture below

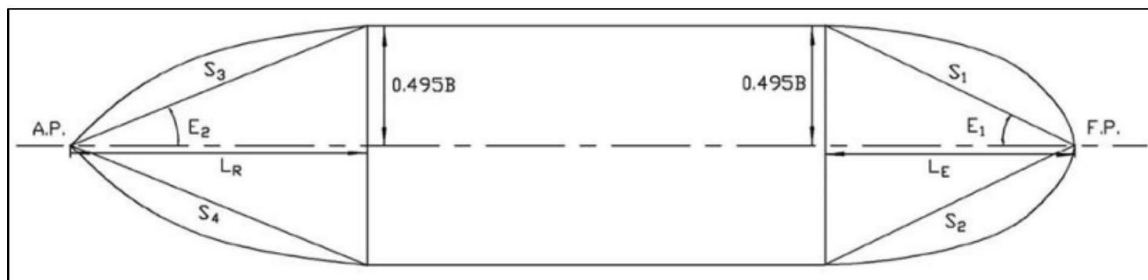


Figure 41: Lengths LR,LE and angles E1,E2 [38, Fig. 15]

B.1.3.2 Ship motion added resistance R_{AWM}

It can be calculated by the formula:

$$R_{AWM} = 4 \cdot \rho \cdot g \cdot \zeta_{\alpha}^2 \cdot \frac{B^2}{L_{pp}} \cdot a_1 \cdot a_2 \cdot a_3 \cdot \bar{\omega}^{b_1} \cdot e^{\frac{b_1 \cdot (1 - \bar{\omega}^{b_1})}{d_1}}$$

Where:

$$a_1 = \begin{cases} 60.3 \cdot C_B^{1.34} \cdot (4 \cdot k_{yy})^2 \cdot \left(\frac{0.87}{C_B}\right)^{-(1+Fr) \cdot \cos \alpha} \cdot \left(\ln \frac{B}{T_{\max}}\right)^{-1} \cdot \frac{(1 - 2 \cdot \cos \alpha)}{3}, & \frac{\pi}{2} \leq \alpha \leq \pi \\ \text{linear interpolation between beam and following seas, } & 0 \leq \alpha \leq \frac{\pi}{2} \\ f(U, V_g), & \alpha = 0 \end{cases}$$

$$V_g = \frac{\sqrt{\frac{g \cdot \lambda}{2 \cdot \pi}}}{2}, \text{ the wave group speed in [m/s]}$$

$$a_2 = \begin{cases} 0.0072 + 0.1676 \cdot Fr, & Fr < 0.12 \\ Fr^{1.5} \cdot e^{-3.5 \cdot Fr}, & Fr \geq 0.12 \end{cases}$$

$$a_3 = 1 + 28.7 \cdot \tanh^{-1} \frac{|T_a - T_f|}{L_{pp}}$$

T_a, T_f : draught at aft and fore respectively in [m]

$$\bar{\omega} = 2.142 \cdot \sqrt[3]{k_{yy}} \cdot \sqrt{\frac{L_{pp}}{\lambda}} \cdot \left[1 - \frac{0.111}{C_B} \cdot \left(\ln \frac{B}{T_{\max}} - \ln 2.75\right)\right] \cdot \left(\frac{C_B}{0.65}\right)^{0.17} \cdot \left[(-1.377 \cdot Fr^2 + 1.157 \cdot Fr) \cdot |\cos \alpha| + \frac{0.618 \cdot (13 + \cos 2\alpha)}{14}\right]$$

k_{yy} : longitudinal mass radius of gyration (pitch)

$$b_1 = \begin{cases} 11, & \bar{\omega} < 1 \\ -8.5, & \text{elsewhere} \end{cases}$$

$$d_1 = \begin{cases} 566 \cdot \left(\frac{L_{pp} \cdot C_B}{B}\right)^{-2.66}, & \bar{\omega} < 1 \\ -566 \cdot \left(\frac{L_{pp}}{B}\right)^{-2.66} \cdot \left(4 - \frac{125 \cdot \tan^{-1}|T_a - T_f|}{L_{pp}}\right), & \text{elsewhere} \end{cases}$$